ASYMPTOTIC COMPATIBILITY OF A CLASS OF NUMERICAL SCHEMES FOR A NONLOCAL TRAFFIC FLOW MODEL*

KUANG HUANG† AND QIANG DU‡

Abstract. This paper considers numerical discretization of a nonlocal conservation law modeling vehicular traffic flows involving nonlocal intervehicle interactions. The nonlocal model involves an integral over the range measured by a horizon parameter and it recovers the local Lighthill—Richards—Whitham model as the nonlocal horizon parameter goes to zero. Good numerical schemes for simulating these parameterized nonlocal traffic flow models should be robust with respect to the change of the model parameters but this has not been systematically investigated in the literature. We fill this gap through a careful study of a class of finite volume numerical schemes with suitable discretizations of the nonlocal integral, which include several schemes proposed in the literature and their variants. Our main contributions are to demonstrate the asymptotically compatibility of the schemes, which includes both the uniform convergence of the numerical solutions to the unique solution of nonlocal continuum model for a given positive horizon parameter and the convergence to the unique entropy solution of the local model as the mesh size and the nonlocal horizon parameter go to zero simultaneously. It is shown that with the asymptotically compatibility, the schemes can provide robust numerical computation under the changes of the nonlocal horizon parameter.

 $\textbf{Key words.} \ \ \text{traffic flow, nonlocal LWR, finite volume schemes, asymptotically compatibility, nonlocal-to-local limit}$

MSC codes. 65M08, 35L65, 76A30, 35R09, 65R20, 65D30

DOI. 10.1137/23M154488X

1. Introduction. In this work, we study the numerical discretization of a non-local analog of the classical Lighthill–Richards–Whitham (LWR) model [42, 44]. The latter, given by

(1.1)
$$\partial_t \rho(t, x) + \partial_x \left(\rho(t, x) v(\rho(t, x)) \right) = 0,$$

for a density $\rho = \rho(t,x)$ and a velocity $v = v(\rho(t,x))$, has been widely used in the study of traffic flows. To study the dynamics of traffic flows in the presence of nonlocal intervehicle interactions [7, 31], the following *nonlocal LWR model* has been developed in recent years:

(1.2)
$$\partial_t \rho(t, x) + \partial_x \left(\rho(t, x) v_\delta(\rho(t, \cdot), t, x) \right) = 0, \quad x \in \mathbb{R}, t > 0.$$

In contrast to (1.1), the nonlocal LWR model (1.2) adopts a modeling assumption that, in a fleet of vehicles driving on a highway, each vehicle decides its driving speed not by the local information but rather through a nonlocal weighted average of traffic information within a road segment of length $\delta > 0$ ahead of the vehicle's current location. More specifically, the velocity $v_{\delta} = v_{\delta}(\rho, t, x)$ takes on the form

^{*}Received by the editors January 3, 2023; accepted for publication (in revised form) December 14, 2023; published electronically May 7, 2024.

https://doi.org/10.1137/23M154488X

Funding: This research is supported in part by US NSF DMS-1937254, DMS-2309245, and CNS-2038984.

[†]Department of Applied Physics and Applied Mathematics, Columbia University, New York, NY 10027 USA. Current affiliation: Department of Mathematics, The Chinese University of Hong Kong, Hong Kong Special Administrative Region, China (kh2862@columbia.edu).

[‡]Department of Applied Physics and Applied Mathematics, and Data Science Institute, Columbia University, New York, NY 10027 USA (qd2125@columbia.edu).

(1.3)

$$v_{\delta}(\rho(t,\cdot),t,x) = v(q_{\delta}(\rho(t,\cdot),t,x)) \quad \text{with} \quad q_{\delta}(\rho(t,\cdot),t,x) = \int_{0}^{\delta} \rho(t,x+s)w_{\delta}(s) \, ds,$$

where the integral kernel $w = w_{\delta}(s)$ is assumed to be a probability density function defined on the interval $[0, \delta]$. Alternatively, one may also consider the nonlocal velocity given by [26]

(1.4)
$$v_{\delta}(\rho(t,\cdot),t,x) = \int_0^{\delta} v(\rho(t,x+s))w_{\delta}(s) ds.$$

The equation (1.2) is solved with the initial condition

$$\rho(0,x) = \rho_0(x), \quad x \in \mathbb{R},$$

where $\rho_0 : \mathbb{R} \to [0, 1]$ represents the initial traffic density. The case $\rho_0 \equiv 0$ indicates that the road is empty, and the case $\rho_0 \equiv 1$ corresponds to fully congested traffic.

The equation (1.2) leads to a nonlocal conservation law due to the nonlocal dependence of the velocity on the density. Consider the rescaled kernel $w_{\delta}(s) = w(s/\delta)/\delta$ such that w_{δ} converges to a Dirac point mass as $\delta \to 0$; it is clear that the nonlocal LWR model (1.2), with either choices of the velocity given by (1.3) or (1.4), formally recovers the local model (1.1) by taking the limit $\delta \to 0$. For more rigorous analysis of the nonlocal LWR model (1.2), we refer to a number of existing studies in the literature, including the model well-posedness [7, 10, 17, 26, 31], traveling wave solutions [45, 48], the asymptotic stability of uniform flows [34], and nonlocal-to-local limit as $\delta \to 0$ [9, 10, 14, 15, 17, 18, 19, 26, 38, 39].

The numerical discretization of the nonlocal LWR model (1.2) has been a subject of interest in numerous studies such as [7, 12, 16, 27, 28, 29, 31]. While these works have introduced a range of numerical schemes, there has been no systematic study on the dependence of numerical solutions on the parameter δ and their behavior under the limit $\delta \to 0$. In the present work, we aim to fill this gap by analysing a class of first-order finite volume schemes for the nonlocal LWR model (1.2). These schemes are designed to correctly resolve both the nonlocal model (1.2) for a given $\delta > 0$ and the local model (1.1) when $\delta \to 0$. Notably, these schemes encompass several from the existing literature and their variants, as detailed in subsection 2.2.

The proposed numerical schemes possess two key components: the numerical flux function that incorporates both local and nonlocal traffic densities and the numerical quadrature weights that are used to evaluate the nonlocal integral in (1.3). We note that the properties of these numerical quadrature weights play an essential role in the behavior of numerical solutions as $\delta \to 0$.

Our main contributions in this work can be summarized as follows. First, we demonstrate that the proposed numerical schemes are monotone, and they share desirable stability properties with monotone schemes for local scalar conservation laws, notably the total variation diminishing (TVD) property. Second, we prove the asymptotic compatibility of the schemes, which includes both the following:

- 1. the convergence of the numerical solution to the unique solution of the nonlocal model (1.2) as the mesh size parameter goes to zero, with the convergence being uniform with respect to the nonlocal horizon parameter $\delta > 0$;
- 2. the convergence of the numerical solution to the unique entropy solution of the local model (1.1) as the mesh size parameter and the nonlocal horizon parameter go to zero simultaneously.

Such asymptotically compatible numerical schemes can offer robust numerical computation under the changes in the nonlocal horizon parameter δ . Discussions on the topic of asymptotically compatible numerical schemes for more general nonlocal models can be found in [51, 52]. Furthermore, we establish the correspondence between local and nonlocal numerical solutions. Specifically, as the nonlocal horizon parameter $\delta \to 0$, the numerical solutions of the nonlocal model (1.2) and the local model (1.1), computed with the same mesh size parameter, approach each other. This convergence is uniform with respect to the mesh size parameter.

The main ingredients of the convergence proofs are the compactness of numerical solutions in the $\mathbf{BV}_{\mathrm{loc}}$ space and their entropy admissibility. Although previous studies such as [7, 31] provided numerical analysis based on a priori \mathbf{L}^{∞} and total variation estimates for numerical solutions with a fixed $\delta > 0$, the resulting total variation bound blows up to infinity as $\delta \to 0$. In this work, a novelty is our use of a different strategy to prove that numerical solutions produced by the proposed numerical schemes satisfy a one-sided Lipschitz condition when δ is close to zero, which enforces both the total variation boundedness and the entropy admissibility of numerical solutions. The strategy we adopt in our analysis bridges prior research in two distinct directions. Firstly, our approach connects to the analysis involving one-sided Lipschitz estimates used in [8, 49] to study numerical schemes for local scalar conservation laws; to our best knowledge, it has not been employed for nonlocal models. Secondly, our approach can provide an alternative proof to the nonlocal-to-local limit of the continuum model as in [17].

Numerical experiments are also reported to complement the theoretical investigation. Note that while the present work is motivated by modeling traffic flows with nonlocal vehicle interactions, let us mention that conservation laws with nonlocal fluxes were also studied in the modeling of pedestrian traffic [11, 20], sedimentation [6], and material flow on conveyor belts [33, 47]; see [1, 4, 5, 13, 21, 25, 30, 37] for more relevant studies. Thus, our study here can be useful in the numerical simulations of a broad range of problems in various application domains.

To summarize the paper, in section 2, after briefly describing the assumptions on the nonlocal model and some basic mathematical properties, we introduce the numerical discretization schemes and summarize the main theorems on their convergence behavior and the asymptotical compatibility. The detailed proofs of the main theorems are given in section 3. We present results of some numerical experiments in section 4 and offer some conclusions in section 5.

2. Preliminaries and main results.

2.1. A review of well-posedness and nonlocal-to-local limit. Let us first state some assumptions on the model.

Assumption 1.

- (i) The nonlocal kernel is given by $w_{\delta}(s) = w(s/\delta)/\delta$ for $s \in [0, \delta]$, where w = w(s) is a \mathbb{C}^1 smooth, strictly decreasing, and nonnegative probability density function defined on [0, 1], and it satisfies the normalization condition $\int_0^1 w(s) \, ds = 1$.
- (ii) The velocity function is $v(\rho) = 1 \rho$. Consequently, (1.3) and (1.4) produce the same outcome.
- (iii) The initial data $\rho_0 \in \mathbf{L}^{\infty}(\mathbb{R})$, and it satisfies $0 \le \rho_0(x) \le 1$ for all $x \in \mathbb{R}$. In addition, ρ_0 has bounded total variation.

Concerning the mathematical analysis of the nonlocal LWR model (1.2), we recall that the existence and uniqueness of weak solutions have been shown with general

choices of the nonlocal kernel, the velocity function, and the initial data; see, for example, [7, 10, 17, 31]. For our case, the following proposition summarizes the known results in the above works.

PROPOSITION 1. Under Assumption 1, the nonlocal LWR model (1.2) admits a unique weak solution $\rho \in \mathbf{L}^{\infty}([0,+\infty) \times \mathbb{R})$ such that

$$(2.1) \int_0^\infty \int_{\mathbb{R}} \rho(t,x) \partial_t \phi(t,x) + \rho(t,x) v_\delta(\rho(t,\cdot),t,x) \partial_x \phi(t,x) \, dx dt + \int_{\mathbb{R}} \rho_0(x) \phi(0,x) \, dx = 0$$

 $\forall \phi \in \mathbf{C}_{\mathrm{c}}^{1}([0,+\infty) \times \mathbb{R}), \text{ where } v_{\delta}(\rho(t,\cdot),t,x) \text{ is given by } (1.3). \text{ Moreover, the solution satisfies the maximum principle}$

(2.2)
$$\inf_{x \in \mathbb{R}} \rho_0(x) \le \rho(t, x) \le \sup_{x \in \mathbb{R}} \rho_0(x), \quad (t, x) \in [0, +\infty) \times \mathbb{R}.$$

The convergence of solutions of the nonlocal LWR model (1.2) as $\delta \to 0$ has also been extensively studied. In the literature, it was usually assumed that the nonlocal kernel $w = w_{\delta}(s)$ is defined for $s \in [0, +\infty)$ and the nonlocal density is defined by

$$q_{\delta}(\rho(t,\cdot),t,x) = \int_{0}^{\infty} \rho(t,x+s) w_{\delta}(s) \, ds.$$

[9, 10] considered the exponential kernels $w_{\delta}(s) = \delta^{-1}e^{-\frac{s}{\delta}}$ and showed convergence from the solutions of the nonlocal model (1.2) to the unique weak entropy solution of the local model (1.1), assuming that the initial data ρ_0 is uniformly positive. [17] generalized the convergence result for a class of nonlocal kernels with exponential decay rate but under one additional assumption that ρ_0 is one-sided Lipschitz continuous. In [17], the authors also provided counterexamples to show that the uniform positivity of the initial data is essential to the convergence result. In the subsequent works [15, 18, 26, 38, 39], convergence results concerning the nonlocal quantity $q_{\delta}(\rho(t,\cdot),t,x)$ as $\delta \to 0$ were given without assuming the initial data being uniformly positive.

In the present work, we adopt an approach similar to that in [17] and make the following additional assumption on the initial data, which basically requires the initial data to be uniformly positive and to have no negative jumps.

Assumption 2. The initial data ρ_0 satisfies

(2.3)
$$\rho_0(x) \ge \rho_{\min} > 0 \quad \forall x \in \mathbb{R}, \qquad -\frac{\rho_0(y) - \rho_0(x)}{y - x} \le L \quad \forall x \ne y \in \mathbb{R},$$

for some constants $\rho_{\min} > 0$ and L > 0.

In our case, the same arguments as in [17] can be applied to give the nonlocal-tolocal limit result, as stated in the following Proposition 2, with very few modifications for compactly supported nonlocal kernels.

PROPOSITION 2. Suppose Assumptions 1 and 2 are satisfied. As $\delta \to 0$, the weak solution of the nonlocal LWR model (1.2) as in Proposition 1 converges in $\mathbf{L}^1_{loc}([0,+\infty)\times\mathbb{R})$ to the weak entropy solution of the local model (1.1) that satisfies

$$(2.4) \int_0^\infty \int_{\mathbb{R}} \rho(t,x) \partial_t \phi(t,x) + \rho(t,x) v\left(\rho(t,x)\right) \partial_x \phi(t,x) \, dx dt + \int_{\mathbb{R}} \rho_0(x) \phi(0,x) \, dx = 0$$

 $\forall \phi \in \mathbf{C}_{c}^{1}([0,+\infty) \times \mathbb{R}), \text{ and }$

$$(2.5) -\frac{\rho(t,y) - \rho(t,x)}{y-x} \le \frac{1}{2t} \quad \forall x \ne y \in \mathbb{R}, \ t > 0.$$

In Proposition 2, the inequality (2.5), which is known as the Oleinik entropy condition, is used to select the unique entropy admissible solution of the scalar conservation law (1.1); see [43]. As a constraint on the one-sided Lipschitz constant of the solution, the entropy condition (2.5) yields that the solution can only have positive jumps.

2.2. Finite volume approximations. Now let us consider the numerical discretization of the nonlocal LWR model (1.2). With finite volume approximations, the numerical solution is defined as a piecewise constant function

(2.6)
$$\rho(t,x) = \sum_{j \in \mathbb{Z}} \sum_{n=0}^{\infty} \rho_j^n \mathbf{1}_{\mathcal{C}_j \times \mathcal{T}^n}(t,x),$$

where $C_j = (x_{j-1/2}, x_{j+1/2})$, $\mathcal{T}^n = (t^n, t^{n+1})$ are spatial and temporal cells. The grid points are $x_j = jh$ and $t^n = n\tau$, where h and τ are spatial and temporal mesh sizes. At the initial time $t^0 = 0$, the initial data is discretized as

(2.7)
$$\rho_j^0 = \frac{1}{h} \int_{\mathcal{C}_j} \rho_0(x) \, dx, \quad j \in \mathbb{Z}.$$

Denote $F_{j-1/2}^n$ and $F_{j+1/2}^n$ the numerical fluxes across cell boundaries at $x_{j-1/2}$ and $x_{j+1/2}$ during time t^n to t^{n+1} . Specifying appropriate numerical fluxes, the finite volume scheme is

(2.8)
$$\rho_j^{n+1} = \rho_j^n + \lambda (F_{j-1/2}^n - F_{j+1/2}^n),$$

where the CFL ratio $\lambda = \tau/h$ is taken to be a fixed constant. To specify the numerical fluxes, we need to evaluate the nonlocal density $q_{\delta}(\rho(t,\cdot),t,x)$ given in (1.3). Let us take

(2.9)
$$q_j^n = \sum_{k=0}^{m-1} w_k \rho_{j+k}^n,$$

where $m = \lceil \frac{\delta}{h} \rceil$ is the number of cells involved in the nonlocal integral, and $\{w_k\}_{k=0}^{m-1}$ is a set of numerical quadrature weights such that

(2.10)
$$w_{\delta,h}(s) = \sum_{k=0}^{m-1} w_k \mathbf{1}_{[kh,(k+1)h)}(s), \quad s \in [0,\delta],$$

is a piecewise constant approximation of the nonlocal kernel $w_{\delta} = w_{\delta}(s)$.

Given the discretized nonlocal densities $\{q_j^n\}_{j\in\mathbb{Z}}^{n\geq 0}$, the nonlocal fluxes in (2.8) can be constructed in a number of different ways. Let us mention the following examples.

• In [7, 31], a Lax–Friedrichs-type scheme was developed with the numerical fluxes

$$F_{j-1/2}^{n} = \frac{1}{2} \left[\rho_{j-1}^{n} v \left(\sum_{k=0}^{m-1} w_{k} \rho_{j+k-1}^{n} \right) + \rho_{j}^{n} v \left(\sum_{k=0}^{m-1} w_{k} \rho_{j+k}^{n} \right) \right] + \frac{\alpha}{2} (\rho_{j-1}^{n} - \rho_{j}^{n}),$$

where $\alpha > 0$ is a numerical viscosity constant, and the numerical quadrature weights are given by the left endpoint values:

(2.12) [Left endpoint]
$$w_k = w_\delta(kh)h$$
, $k = 0, \dots, m-1$.

In [28], a Godunov-type scheme was proposed with the numerical fluxes defined by

(2.13)
$$F_{j-1/2}^{n} = \rho_{j-1}^{n} v \left(\sum_{k=0}^{m-1} w_k \rho_{j+k}^{n} \right),$$

where the numerical quadrature weights are given by the exact quadrature:

(2.14)

[Exact quadrature]
$$w_k = \int_{kh}^{\min\{(k+1)h,\delta\}} w_{\delta}(s) ds$$
, $k = 0, \dots, m-1$.

• Inspired by both (2.11) and (2.13), we also consider the following Lax–Friedrichs-type fluxes:

(2.15)
$$F_{j-1/2}^{n} = \frac{1}{2} \left(\rho_{j-1}^{n} + \rho_{j}^{n} \right) v \left(\sum_{k=0}^{m-1} w_{k} \rho_{j+k}^{n} \right) + \frac{\alpha}{2} (\rho_{j-1}^{n} - \rho_{j}^{n}),$$

where the numerical quadrature weights are given by either the left endpoint values or the exact quadrature.

In the present work, we consider a family of finite volume schemes:

(2.16)
$$\rho_j^{n+1} = \mathcal{H}\left(\rho_{j-1}^n, \rho_j^n, \rho_{j+1}^n, \dots, \rho_{j+m}^n\right) = \rho_j^n + \lambda(F_{j-1/2}^n - F_{j+1/2}^n),$$

$$(2.17) \hspace{3.1em} = \rho_j^n + \lambda \left[g(\rho_{j-1}^n, \rho_j^n, q_{j-1}^n, q_j^n) - g(\rho_j^n, \rho_{j+1}^n, q_j^n, q_{j+1}^n) \right],$$

where q_j^n is given by (2.9), $\lambda = \tau/h$ is the CFL ratio, and $g = g(\rho_L, \rho_R, q_L, q_R)$ is a numerical flux function that depends on both local densities ρ_L, ρ_R and nonlocal densities q_L, q_R . We remark that, by taking $q_L = \rho_L$ and $q_R = \rho_R$, $g = g(\rho_L, \rho_R, \rho_L, \rho_R)$ becomes a numerical flux function for the local model (1.1), and the respective numerical scheme,

$$(2.18) \rho_j^{n+1} = \rho_j^n + \lambda \left[g(\rho_{j-1}^n, \rho_j^n, \rho_{j-1}^n, \rho_j^n) - g(\rho_j^n, \rho_{j+1}^n, \rho_j^n, \rho_{j+1}^n) \right],$$

can be viewed as the local counterpart of (2.16)–(2.17).

In the present work, we make the following assumptions on the numerical quadrature weights, the numerical flux function, and the CFL ratio λ .

Assumption 3. The numerical quadrature weights $\{w_k\}_{k=0}^{m-1}$ satisfy

$$w_{\delta}(kh)h \ge w_k \ge w_{\delta}((k+1)h)h$$
 and $w_k - w_{k+1} \ge c(h/\delta)^2$, $k = 0, \dots, m-1$,

for some constant c > 0 only depending on the kernel function w = w(s), where we make the convention that $w_m = 0$. Moreover, $\{w_k\}_{k=0}^{m-1}$ satisfy the normalization condition:

(2.20)
$$\sum_{k=0}^{m-1} w_k = 1.$$

Assumption 4. (i) The numerical flux function g is a quadratic polynomial, and it is separately affine in all of its arguments. (ii) When $\rho_L = \rho_R$ and $q_L = q_R$, $g(\rho_L, \rho_L, q_L, q_L) = \rho_L (1 - q_L)$. (iii) Denote γ_{ij} , $1 \le i, j \le 4$ as the second-order partial derivatives of g; they satisfy

$$(2.21) \gamma_{11} = \gamma_{12} = \gamma_{22} = 0, \quad \gamma_{33} = \gamma_{34} = \gamma_{44} = 0,$$

$$(2.22) \gamma_{13}, \gamma_{23}, \gamma_{14}, \gamma_{24} \le 0, \quad \gamma_{13} + \gamma_{23} + \gamma_{14} + \gamma_{24} = -1.$$

(iv) Denote $\theta^{(i)}$, $1 \le i \le 4$ as the first-order partial derivatives of g with respect to its four arguments ρ_L , ρ_R , q_L , q_R . For any $0 \le \rho_L$, ρ_R , q_L , $q_R \le 1$,

$$(2.23) \theta^{(1)}(q_L, q_R) \ge 0, \ \theta^{(2)}(q_L, q_R) \le 0, \ \theta^{(3)}(\rho_L, \rho_R) \le 0, \ \theta^{(4)}(\rho_L, \rho_R) \le 0,$$

$$(2.24) \quad \theta^{(1)}(q_L, q_R) + \theta^{(3)}(\rho_L, \rho_R) + 2(\gamma_{13} + \gamma_{23}) \ge 0, \quad \theta^{(2)}(q_L, q_R) - 2(\gamma_{23} + \gamma_{24}) \le 0,$$

(2.25)
$$\theta^{(3)}(\rho_L, \rho_R) + \theta^{(4)}(\rho_L, \rho_R) \le -\min\{\rho_L, \rho_R\}.$$

We note that due to (2.21), the partial derivatives in Assumption 4 can be expressed as functions of a pair of variables only, instead of all four variables.

Assumption 5. Given the notation $\theta^{(i)}$, $1 \le i \le 4$ in Assumption 4, λ satisfies

(2.26)
$$\lambda \left(\sum_{i=1}^{4} \left\| \theta^{(i)} \right\|_{\infty} + 3 \right) \le 1.$$

It is worthwhile to mention that the aforementioned schemes, with numerical fluxes in (2.11), (2.13), and (2.15), all belong to the family (2.16)–(2.17) with the numerical flux functions given by

(2.27a)
$$[\text{Lax - Friedrichs}] \quad g(\rho_L, \rho_R, q_L, q_R) = \frac{1}{2} (\rho_L v(q_L) + \rho_R v(q_R)) \\ + \frac{\alpha}{2} (\rho_L - \rho_R),$$

(2.27b)
$$[Godunov] \quad g(\rho_L, \rho_R, q_L, q_R) = \rho_L v(q_R),$$

(2.27c) [modifiedLax – Friedrichs]
$$g(\rho_L, \rho_R, q_L, q_R) = \frac{1}{2}(\rho_L + \rho_R)v(q_R) + \frac{\alpha}{2}(\rho_L - \rho_R),$$

respectively. Moreover, let us mention that the numerical flux functions given above all satisfy the Assumption 4. The proof of the following proposition is through direct calculation, and we will omit the details here.

PROPOSITION 3. The Godunov-type flux function (2.27b) satisfies the Assumption 4. The Lax-Friedrichs-type numerical flux functions (2.27a) and (2.27c) both satisfy the Assumption 4, provided that the numerical viscosity constant $\alpha \geq 3$.

Let us make some additional remarks concerning Assumption 4 for the numerical flux function g. Considering the velocity function $v(\rho) = 1 - \rho$, the flux function in the continuum model (1.2) is $\rho(1-q)$, which is a quadratic polynomial in ρ, q with the sole quadratic term being $-\rho q$. Therefore, it is reasonable to assume that the

numerical flux function g is quadratic with its second-order derivatives satisfying the condition (ii). The condition (ii) ensures the consistency of the scheme (2.16)–(2.17) with the model (1.2), while the condition (iv) is utilized to show that the scheme is monotone under all Assumptions 1–5, as seen in Theorem 1. It is natural to ask if the results in this work can be extended to more general numerical flux functions, where g may not be a quadratic polynomial. We leave the study of such an extension to future works [2, 3].

Furthermore, we leave detailed discussions about the selection of numerical quadrature weights to subsection 2.4, where we also provide candidates that satisfy the Assumption 3.

- **2.3.** Main results. This section summarizes the main results. We note that all the theorems are subject to Assumptions 1–5. To clarify the notation, we denote the following:
 - ρ^{δ} : the continuous solution of the nonlocal LWR model (1.2);
 - ρ^0 : the continuous solution of the local LWR model (1.1);
 - $\rho^{\delta,h}$: the numerical solution of the nonlocal LWR model; and
 - $\rho^{0,h}$: the numerical solution of the local LWR model.

There are two parameters: the nonlocal horizon parameter δ and the mesh size parameter h. In the present work, we are interested in establishing relations between those solutions when $\delta \to 0$ and $h \to 0$ along various limiting paths, as shown in Figure 2.1.

The following convergence results are given or readily established.

- 1. The numerical convergence for the nonlocal model: $\rho^{\delta,h} \to \rho^{\delta}$ when $h \to 0$ with fixed $\delta > 0$ can be proved following the approach in [31]. The proof is based on a priori \mathbf{L}^{∞} and total variation estimates of the numerical solution.
- 2. The numerical convergence for the local model: $\rho^{0,h} \to \rho^0$ when $h \to 0$ is a classical result; see, for example [32].
- 3. The nonlocal-to-local limit: $\rho^{\delta} \to \rho^{0}$ when $\delta \to 0$ is given in Proposition 2.

One of our key contributions is to prove the asymptotic compatibility of the proposed scheme (2.16)–(2.17), which includes both

- 1. the convergence $\rho^{\delta,h} \to \rho^0$ as both $\delta \to 0$ and $h \to 0$ simultaneously; see Theorem 2; and
- 2. the numerical convergence $\rho^{\delta,h} \to \rho^{\delta}$ as $h \to 0$ uniformly in δ ; see Theorem 3. The proofs of these two theorems rely on the stability estimates provided in Theorem 1.

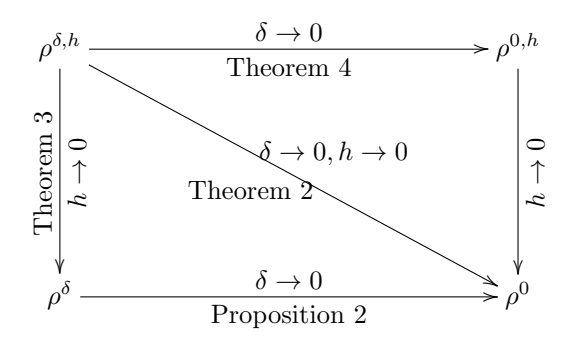


Fig. 2.1. Diagram of various limiting paths.

THEOREM 1. Under Assumptions 1-5, and taking that

$$(2.28) 0 < \delta \le \delta_0 \doteq \frac{c\rho_{\min}}{2w(0)L},$$

where the constant c is as in (2.19) and the constants ρ_{\min} and L are as in (2.3), the numerical solution $\rho^{\delta,h}$ produced by the scheme (2.16)–(2.17) satisfies the maximum principle

(2.29)
$$\inf_{x \in \mathbb{R}} \rho_0(x) \le \rho^{\delta,h}(t,x) \le \sup_{x \in \mathbb{R}} \rho_0(x), \quad (t,x) \in [0,+\infty) \times \mathbb{R}.$$

Moreover, the scheme (2.16)–(2.17) is monotone, meaning that the function \mathcal{H} defined in (2.16)–(2.17) is nondecreasing with respect to each of its arguments. Consequently, the spatial total variation of the numerical solution $\mathrm{TV}(\rho^{\delta,h}(t,\cdot))$ is a nonincreasing function of time $t \in [0,+\infty)$.

THEOREM 2. Under Assumptions 1–5, when $\delta \to 0$ and $h \to 0$ simultaneously, the numerical solution $\rho^{\delta,h}$ produced by the scheme (2.16)–(2.17) converges in $\mathbf{L}^1_{loc}([0,+\infty) \times \mathbb{R})$ to the weak entropy solution ρ^0 of the local model (1.1) as defined in Proposition 2.

THEOREM 3. Under Assumptions 1–5, and taking that δ satisfies the condition (2.28), as $h \to 0$, the numerical solution $\rho^{\delta,h}$ produced by the scheme (2.16)–(2.17) converges in $\mathbf{L}^1_{loc}([0,+\infty)\times\mathbb{R})$ to the weak solution ρ^{δ} of the nonlocal model (1.2) as defined in Proposition 1. Moreover, the convergence is uniform with respect to $\delta \in (0,\delta_0]$, where δ_0 is as in (2.28):

$$\lim_{h\to 0} \sup_{\delta\in(0,\delta_0]} \|\rho^{\delta,h} - \rho^{\delta}\|_{\mathbf{L}^1(U)} = 0, \quad \text{for any bounded domain } U \subset [0,+\infty) \times \mathbb{R}.$$

Let us provide some remarks on the convergence rates in the above Theorem 2 and Theorem 3. On one hand, the scheme (2.16)–(2.17) is expected to be at most first-order accurate because it is based on a piecewise constant approximation. On the other hand, for local scalar conservation laws, it is known that the convergence rate may drop to half-order for discontinuous solutions [41]. In the numerical experiments in section 4, we test the scheme with both smooth initial data and piecewise constant ones; the results validate the first-order convergence rate to the local solution (as in Theorem 2) when $\delta = mh$ for a fixed integer m > 0 and the first-order convergence rate to the nonlocal solution uniformly in δ (as in Theorem 3). For convergence to the local solution, this linear convergence behavior is consistent with that observed and rigorously proved in [50] for monotone schemes for local scalar conservation laws when the initial data is piecewise constant and fulfills Oleinik's entropy condition. The rigorous analysis of convergence rates along various limiting paths may require Kuznetsov-type arguments as outlined in [2, 3]. We leave this for future research.

Finally, we establish the correspondence between the nonlocal numerical solution $\rho^{\delta,h}$ and the local numerical solution $\rho^{0,h}$, as outlined in Theorem 4. In the case where h is fixed, the theorem asserts that $\rho^{\delta,h}$ and $\rho^{0,h}$ are indeed identical whenever $0 < \delta < h$, meaning that the nonlocal horizon is within a single spatial mesh cell. In the case where h is also taken to approach zero, the theorem establishes the uniform convergence for $h \in (0, \delta]$, as detailed in (2.32). This feature aligns with the principle behind asymptotic preserving schemes [24, 35, 36], which are designed to incorporate the asymptotic behavior of continuous solutions into numerical schemes. In the context of this work, this property signifies that the numerical solution preserves the

limiting behavior of the continuous solution of the nonlocal model as the nonlocal horizon parameter $\delta \to 0$.

THEOREM 4. Under Assumptions 1–5, let $\rho^{\delta,h}$ be the numerical solution produced by the scheme (2.16)–(2.17) and $\rho^{0,h}$ be the one produced by (2.18). It holds that

(2.31)
$$\rho^{\delta,h} = \rho^{0,h} \quad \text{when} \quad 0 < \delta < h.$$

Moreover,

(2.32)

$$\lim_{\delta \to 0} \sup_{0 < h < \delta} \left\| \rho^{\delta,h} - \rho^{0,h} \right\|_{\mathbf{L}^1(U)} = 0, \quad \text{for any bounded domain } U \subset [0,+\infty) \times \mathbb{R}.$$

2.4. Comments on numerical quadrature weights. Let us make some remarks on the choice of the numerical quadrature weights $\{w_k\}_{k=0}^{m-1}$. Provided that the nonlocal kernel $w_{\delta} = w_{\delta}(s)$ is \mathbf{C}^1 smooth and decreasing, one can write the numerical quadrature weights as

$$w_k = w(\xi_k) \frac{h}{\delta}, \quad \xi_k \in \left[k \frac{h}{\delta}, (k+1) \frac{h}{\delta} \right], \quad k = 0, \dots, m-1,$$

where $\{\xi_k\}_{0\leq k\leq m-1}$ can be viewed as sampling points of a Riemann sum quadrature on [0,1].

The condition (2.19) in Assumption 3 basically requires that the sampling points should not be too close to each other, and the condition is used to derive the necessary a priori estimates on numerical solutions as in Theorem 1. To demonstrate the meaning of the constant c and the factor $(h/\delta)^2$ in (2.19), let us illustrate with the left endpoint quadrature weights in (2.12). In this case,

$$w_{k-1} - w_k = \frac{h}{\delta} \left[w \left((k-1) \frac{h}{\delta} \right) - w \left(k \frac{h}{\delta} \right) \right] \ge c \left(\frac{h}{\delta} \right)^2,$$

where the constant $c = \min_{s \in [0,1]} -w'(s) > 0$.

The condition (2.20) in Assumption 3 is the normalization condition for the numerical quadrature weights, which is essential to the consistency between the scheme (2.16)–(2.17) and the local model (1.1). To demonstrate potential risks when the normalization condition (2.20) is violated, let us consider the case $\delta = mh$, where m is a fixed positive integer. Then the scheme (2.16)–(2.17) can be viewed as a m + 2-point conservative scheme of the local model (1.1) with the numerical flux function

$$g_{\text{local}}(\rho_j, \dots, \rho_{j+m}) = g\left(\rho_j, \rho_{j+1}, \sum_{k=0}^{m-1} w_k \rho_{j+k}, \sum_{k=0}^{m-1} w_k \rho_{j+k+1}\right),$$

where g is as in Assumption 4. Suppose $\rho_j = \cdots = \rho_{j+m} = \bar{\rho}$; to make g_{local} consistent to the local model (1.1), it is necessary to have

$$g_{\text{local}}(\bar{\rho},\ldots,\bar{\rho}) = \bar{\rho}\left(1 - \bar{\rho}\sum_{k=0}^{m-1} w_k\right) = \bar{\rho}(1 - \bar{\rho}),$$

which requires the normalization condition (2.20). In contrast, if the condition (2.20) is violated and $\eta \doteq \sum_{k=0}^{m-1} w_k \neq 1$, the numerical solutions will formally converge to a solution of the equation

$$\partial_t \rho(t,x) + \partial_x (\rho(t,x)(1-\eta\rho(t,x))) = 0.$$

other than the desired equation (1.1) with $v(\rho) = 1 - \rho$. This means that the absence of the normalization condition (2.20) for some numerical quadrature weights may lead to incorrect limit solutions when $\delta \to 0$ and $h \to 0$ simultaneously. Hence, we introduce the following normalized left endpoint quadrature weights:

$$(2.33) \qquad [\text{Normalized left endpoint}] \quad w_k = \frac{w_\delta(kh)h}{\sum_{k=0}^{m-1} w_\delta(kh)h}, \quad k = 0, \dots, m-1,$$

and give the following proposition.

PROPOSITION 4. The normalized left endpoint quadrature weights (2.33) and the exact quadrature weights (2.14) both satisfy the Assumption 3, with the constant c in the condition (2.19) given by $c = \frac{1}{1+w(0)} \min_{s \in [0,1]} -w'(s)$ and $c = \frac{1}{2} \min_{s \in [0,1]} -w'(s)$, respectively. The left endpoint quadrature weights satisfy the condition (2.19) with the constant $c = \min_{s \in [0,1]} -w'(s)$, but they do not satisfy the normalization condition (2.20).

A comparison between different choices of numerical quadrature weights is made through numerical experiments in section 4.

- **3. Proof of theorems.** This section aims to give the proofs of our main results. First, in subsection 3.1, we establish the maximum principle for numerical solutions. Then we present a one-sided Lipschitz estimate for numerical solutions in subsection 3.2; the monotonicity of the numerical scheme (2.16)-(2.17) and its TVD property follow as corollaries. These two subsections together constitute the proof of Theorem 1. In subsection 3.3, we consider the limit as $h \to 0$ and demonstrate convergence of numerical solutions to the proper nonlocal or local solution, which provides the proofs of Theorem 2 and Theorem 3. In subsection 3.4, we offer the proof of Theorem 4 concerning the nonlocal-to-local limit of numerical discretizations.
- **3.1. Maximum principle.** In this subsection, we aim to show the maximum principle (2.29) in Theorem 1. By Assumption 1 and (2.7), the numerical solution at the initial time $\{\rho_j^0\}_{j\in\mathbb{Z}}$ satisfies $0\leq \rho_j^0\leq 1$ for all $j\in\mathbb{Z}$. Then the maximum principle (2.29) can be proved by induction using the following Lemma 1.

Lemma 1. Suppose all conditions in Theorem 1 are met and that $0 \le \rho_{\min} \le \rho_{j+k}^n \le \rho_{\max} \le 1$ for $k=-1,0,1,\ldots,m$. Then we have

(3.1)
$$\rho_{\min} \leq \mathcal{H}(\rho_{j-1}^n, \rho_j^n, \rho_{j+1}^n, \dots, \rho_{j+m}^n) \leq \rho_{\max},$$

where the function \mathcal{H} is as defined in (2.16)-(2.17).

Let us first check the monotonicity of the scheme defined by (2.16)–(2.17). Denote $\theta_j^{n,(i)} = \theta^{(i)}(q_{j-1}^n, q_j^n), \ i = 1, 2; \quad \theta_j^{n,(i)} = \theta^{(i)}(\rho_{j-1}^n, \rho_j^n), \ i = 3, 4 \quad \text{for} \quad j \in \mathbb{Z}, \ n \geq 0.$

A direct calculation gives

$$(3.2a) \quad \frac{\partial \mathcal{H}}{\partial \rho_{j-1}^{n}} = \lambda \left(\theta_{j}^{n,(1)} + w_{0} \theta_{j}^{n,(3)} \right);$$

$$(3.2b) \quad \frac{\partial \mathcal{H}}{\partial \rho_{j}^{n}} = 1 + \lambda \left(\theta_{j}^{n,(2)} - \theta_{j+1}^{n,(1)} + w_{1} \theta_{j}^{n,(3)} + w_{0} \theta_{j}^{n,(4)} - w_{0} \theta_{j+1}^{n,(3)} \right);$$

$$(3.2c) \quad \frac{\partial \mathcal{H}}{\partial \rho_{j+1}^{n}} = \lambda \left(-\theta_{j+1}^{n,(2)} + w_{2} \theta_{j}^{n,(3)} - w_{1} \theta_{j+1}^{n,(3)} + w_{1} \theta_{j}^{n,(4)} - w_{0} \theta_{j+1}^{n,(4)} \right);$$

$$(3.2d) \quad \frac{\partial \mathcal{H}}{\partial \rho_{j+k}^{n}} = \lambda \left(w_{k+1} \theta_{j}^{n,(3)} - w_{k} \theta_{j+1}^{n,(3)} + w_{k} \theta_{j}^{n,(4)} - w_{k-1} \theta_{j+1}^{n,(4)} \right), \quad k = 2, \dots, m;$$

where we make the convention that $w_m = w_{m+1} = 0$.

In (3.2d), which corresponds to the nonlocal dependence of the flux on the solution, it is possible that $\theta_j^{n,(3)} < 0$, $\theta_j^{n,(4)} < 0$ while $\theta_{j+1}^{n,(3)} = \theta_{j+1}^{n,(4)} = 0$ at some point $j = j_0$, e.g., if we consider the Riemann-type solution:

$$\rho_j^n = 1, \ j \le j_0; \quad \rho_j^n = 0, \ j > j_0.$$

In this case, $\frac{\partial \mathcal{H}}{\partial \rho_{j+k}^n} < 0$ for k = 2, ..., m-1. Therefore, one can not deduce (3.1) by showing (2.16)–(2.17) is a monotone scheme. Here we prove (3.1) in an alternative way, which was also used in [28, 31].

Proof of Lemma 1. We observe the identity $\mathcal{H}(\rho_{\min}, \rho_{\min}, \rho_{\min}, \rho_{\min}, \dots, \rho_{\min}) = \rho_{\min}$; thus we can write the term $\mathcal{H}(\rho_{j-1}^n, \rho_j^n, \rho_{j+1}^n, \dots, \rho_{j+m}^n) - \rho_{\min}$ as the summation of two parts:

$$\Delta \mathcal{H}_1 = \mathcal{H}(\rho_{j-1}^n, \rho_j^n, \rho_{j+1}^n, \rho_{j+2}^n, \dots, \rho_{j+m}^n) - \mathcal{H}(\rho_{\min}, \rho_{\min}, \rho_{j+1}^n, \rho_{j+2}^n, \dots, \rho_{j+m}^n),$$

$$\Delta \mathcal{H}_2 = \mathcal{H}(\rho_{\min}, \rho_{\min}, \rho_{j+1}^n, \rho_{j+2}^n, \dots, \rho_{j+m}^n) - \mathcal{H}(\rho_{\min}, \rho_{\min}, \rho_{\min}, \rho_{\min}, \rho_{\min}, \dots, \rho_{\min}).$$

By the mean value theorem,

$$\Delta \mathcal{H}_{1} = \sum_{k=-1,0} \frac{\partial \mathcal{H}}{\partial \rho_{j+k}^{n}} (\tilde{\rho}_{j-1}^{n}, \tilde{\rho}_{j}^{n}, \rho_{j+1}^{n}, \rho_{j+2}^{n}, \dots, \rho_{j+m}^{n}) (\rho_{j+k}^{n} - \rho_{\min}),$$

$$\Delta \mathcal{H}_{2} = \sum_{1 \leq k \leq m} \frac{\partial \mathcal{H}}{\partial \rho_{j+k}^{n}} (\rho_{\min}, \rho_{\min}, \tilde{\rho}_{j+1}^{n}, \tilde{\rho}_{j+2}^{n}, \dots, \tilde{\rho}_{j+m}^{n}) (\rho_{j+k}^{n} - \rho_{\min}),$$

where $0 \le \rho_{\min} \le \tilde{\rho}_{j+k}^n \le \rho_{\max} \le 1 \ \forall k = -1, 0, 1, \dots, m$.

Let us use (3.2a)–(3.2d) with $\theta_j^{n,(i)}$ replaced by $\tilde{\theta}_j^{n,(i)}$ that is with respect to $\tilde{\rho}_{j+k}^n$. By Assumption 4, we have $\tilde{\theta}_j^{n,(1)} + w_0 \tilde{\theta}_j^{n,(3)} \geq \tilde{\theta}_j^{n,(1)} + \tilde{\theta}_j^{n,(3)} \geq 0$ given that the term with respect to k=1 in $\Delta \mathcal{H}_1$ is nonnegative. Moreover, Assumption 5 implies that the term with respect to k=0 in $\Delta \mathcal{H}_1$ is nonnegative. For $\Delta \mathcal{H}_2$, we note that

$$\begin{split} \tilde{\theta}_{j+1}^{n,(3)} &= \tilde{\theta}_{j}^{n,(3)} + \gamma_{23} (\tilde{\rho}_{j+1}^{n} - \rho_{\min}) \leq \tilde{\theta}_{j}^{n,(3)}, \\ \tilde{\theta}_{j+1}^{n,(4)} &= \tilde{\theta}_{j}^{n,(4)} + \gamma_{24} (\tilde{\rho}_{j+1}^{n} - \rho_{\min}) \leq \tilde{\theta}_{j}^{n,(4)}, \end{split}$$

which yields that

$$\begin{split} w_{k+1}\tilde{\theta}_{j}^{n,(3)} - w_{k}\tilde{\theta}_{j+1}^{n,(3)} + w_{k}\tilde{\theta}_{j}^{n,(4)} - w_{k-1}\tilde{\theta}_{j+1}^{n,(4)} &\geq (w_{k+1} - w_{k})\tilde{\theta}_{j}^{n,(3)} \\ &+ (w_{k} - w_{k-1})\tilde{\theta}_{j}^{n,(4)} &\geq 0, \end{split}$$

for k = 1, ..., m. As a consequence, all terms in $\Delta \mathcal{H}_2$ are nonnegative. Then we deduce that

$$\mathcal{H}(\rho_{j-1}^n, \rho_j^n, \rho_{j+1}^n, \dots, \rho_{j+m}^n) - \rho_{\min} = \Delta \mathcal{H}_1 + \Delta \mathcal{H}_2 \ge 0.$$

Similarly one can show the upper bound estimate $\mathcal{H}(\rho_{j-1}^n, \rho_j^n, \rho_{j+1}^n, \dots, \rho_{j+m}^n) - \rho_{\max} \leq 0$.

3.2. One-sided Lipschitz estimate. This section aims to derive a one-sided Lipschitz estimate for numerical solutions as given in Lemma 2 and Lemma 3. Utilizing the one-sided Lipschitz estimate, we proceed to establish that the scheme (2.16)–(2.17) is monotone and TVD, as demonstrated in Lemma 4 and Lemma 5.

LEMMA 2. Suppose that all conditions in Theorem 1 are met and that $\{\rho_j^n\}_{j\in\mathbb{Z}}^{n\geq 0}$ is the numerical solution produced by the scheme (2.16)–(2.17). The numerical differences

(3.3)
$$r_{i}^{n} = \rho_{i+1}^{n} - \rho_{i}^{n}, \quad j \in \mathbb{Z}, \ n \ge 0,$$

satisfy

(3.4)
$$r_i^n \ge -Lh, \quad j \in \mathbb{Z}, \ n \ge 0,$$

where the constant L is as in (2.3).

Proof. It follows from the definition of the scheme (2.16)–(2.17) that

$$(3.5) \\ r_j^{n+1} = r_j^n + \lambda \left[2g(\rho_j^n, \rho_{j+1}^n, q_j^n, q_{j+1}^n) - g(\rho_{j-1}^n, \rho_j^n, q_{j-1}^n, q_j^n) - g(\rho_{j+1}^n, \rho_{j+2}^n, q_{j+1}^n, q_{j+2}^n) \right].$$

Noting that g is a quadratic polynomial, we see that $g(\rho_j^n,\rho_{j+1}^n,q_j^n,q_{j+1}^n)-g(\rho_{j-1}^n,\rho_j^n,q_{j-1}^n,q_j^n)$ and $g(\rho_{j+1}^n,\rho_{j+2}^n,q_{j+1}^n,q_{j+2}^n)-g(\rho_{j-1}^n,\rho_j^n,q_{j-1}^n,q_j^n)$ can be expressed, respectively, as linear combinations of the differences $\{\rho_j^n-\rho_{j-1}^n=r_{j-1}^n,\rho_{j+1}^n-\rho_j^n=r_j^n,q_{j-1}^n-q_{j-1}^n,q_{j+1}^n-q_j^n\}$ and $\{\rho_{j+1}^n-\rho_{j-1}^n=r_j^n+r_{j-1}^n,\rho_{j+2}^n-\rho_j^n=r_{j+1}^n+r_j^n,q_{j+1}^n-q_{j-1}^n=q_{j+1}^n-q_j^n+q_j^n-q_{j-1}^n,q_{j+2}^n-q_j^n=q_{j+2}^n-q_{j+1}^n+q_{j+1}^n-q_j^n\}$, with the coefficients of the linear combinations dependent on the first- and second-order partial derivatives introduced in the Assumption 4. This leads to

$$\begin{split} (3.6) \ \ r_{j}^{n+1} &= \lambda \theta_{j}^{n,(1)} r_{j-1}^{n} + \left(1 + \lambda \theta_{j}^{n,(2)} - \lambda \theta_{j}^{n,(1)}\right) r_{j}^{n} - \lambda \theta_{j}^{n,(2)} r_{j+1}^{n} \\ &\quad + \lambda \left(\theta_{j}^{n,(3)} + \sigma_{j-1}^{n}\right) (q_{j}^{n} - q_{j-1}^{n}) \\ &\quad + \lambda \left(\theta_{j}^{n,(4)} - \theta_{j}^{n,(3)} + \sigma_{j}^{n}\right) (q_{j+1}^{n} - q_{j}^{n}) - \lambda \left(\theta_{j}^{n,(4)} + \sigma_{j+1}^{n}\right) (q_{j+2}^{n} - q_{j+1}^{n}), \end{split}$$

where $\{\theta_j^{n,(i)}=\theta^{(i)}(q_{j-1}^n,q_j^n)\}_{i=1}^2,\ \{\theta_j^{n,(i)}=\theta^{(i)}(\rho_{j-1}^n,\rho_j^n)\}_{i=3}^4$ for $j\in\mathbb{Z}$ and $n\geq 0$, and

(3.7a)
$$\sigma_{j-1}^n = \gamma_{13}r_{j-1}^n + (\gamma_{23} - \gamma_{13})r_j^n - \gamma_{23}r_{j+1}^n,$$

(3.7b)
$$\sigma_j^n = (\gamma_{14} - \gamma_{13})r_{j-1}^n + (\gamma_{24} - \gamma_{13} - \gamma_{14} - \gamma_{23})r_j^n - (\gamma_{23} + \gamma_{24})r_{j+1}^n,$$

(3.7c)
$$\sigma_{j+1}^n = \gamma_{14}r_{j-1}^n + (\gamma_{14} + \gamma_{24})r_j^n + \gamma_{24}r_{j+1}^n.$$

Moreover, the definition in (2.9) gives $q_{j+1}^n - q_j^n = \sum_{k=0}^{m-1} w_k r_{j+k}^n$ for $j \in \mathbb{Z}$ and $n \ge 0$. Upon substituting it in (3.6) and carefully regroup terms, we see that r_j^{n+1} can be expressed as a combination of $\{r_{j+k}^n\}_{k=-1}^m$ plus two extra nonnegative quadratic terms involving $(r_j^n)^2$ and $(r_{j+1}^n)^2$. That is,

$$(3.8) r_j^{n+1} = \sum_{-1 \le k \le m} c_{j,k}^n r_{j+k}^n - 2\lambda(\gamma_{13} + \gamma_{14})(r_j^n)^2 - 2\lambda(\gamma_{23} + \gamma_{24})(r_{j+1}^n)^2,$$

with $\sum_{-1 \le k \le m} c_{j,k}^n = 1$, where the coefficients $\{c_{j,k}^n\}_{-1 \le k \le m}$ are given by

$$\begin{split} c^n_{j,-1} &= \lambda \theta^{n,(1)}_j + \lambda w_0 \left(\theta^{n,(3)}_j + \sigma^n_{j-1} \right); \\ c^n_{j,0} &= 1 + \lambda \left(\theta^{n,(2)}_j - \theta^{n,(1)}_j \right) + \lambda w_1 \left(\theta^{n,(3)}_j + \sigma^n_{j-1} \right) + \lambda w_0 \left(\theta^{n,(4)}_j - \theta^{n,(3)}_j + \sigma^n_j \right) \\ &\quad + 2\lambda (\gamma_{13} + \gamma_{14}) r^n_j; \\ c^n_{j,1} &= -\lambda \theta^{n,(2)}_j + \lambda \left[w_2 \left(\theta^{n,(3)}_j + \sigma^n_{j-1} \right) + w_1 \left(\theta^{n,(4)}_j - \theta^{n,(3)}_j + \sigma^n_j \right) \right. \\ &\quad - w_0 \left(\theta^{n,(4)}_j + \sigma^n_{j+1} \right) \right] + 2\lambda (\gamma_{23} + \gamma_{24}) r^n_{j+1}; \\ c^n_{j,m} &= -\lambda w_{m-1} \left(\theta^{n,(4)}_j + \sigma^n_{j+1} \right); \quad \text{and for } 2 \leq k \leq m-1, \text{ with } w_m = 0, \\ c^n_{j,k} &= \lambda \left[w_{k+1} \left(\theta^{n,(3)}_j + \sigma^n_{j-1} \right) + w_k \left(\theta^{n,(4)}_j - \theta^{n,(3)}_j + \sigma^n_j \right) - w_{k-1} \left(\theta^{n,(4)}_j + \sigma^n_{j+1} \right) \right]. \end{split}$$

Since the one-sided Lipschitz condition in (2.3) gives $r_j^0 \ge -Lh \ \forall j \in \mathbb{Z}$, we proceed by induction to show the claim that $r_j^n \ge -Lh$ for $j \in \mathbb{Z}$ and $n \ge 0$ and the coefficients $\{c_{j,k}^n\}_{-1 \le k \le m}$ in (3.8) are all nonnegative, under Assumptions 1–5.

We note that the maximum principle of the numerical solution as given in (2.29) implies the estimate $|r_i^n| \le 1$ for all $j \in \mathbb{Z}$ and $n \ge 0$. Then we obtain that

$$\begin{split} c_{j,-1}^n &\geq \lambda \left(\theta_j^{n,(1)} + \theta_j^{n,(3)} - 2(\gamma_{13} + \gamma_{23}) \right) \geq 0, \\ c_{j,0}^n &\geq 1 - \lambda \left(\sum_{i=1}^4 \left| \theta_j^{n,(i)} \right| - 2(\gamma_{13} + \gamma_{23} + \gamma_{14} + \gamma_{24}) \right) \\ &\geq 1 - \lambda \left(\sum_{i=1}^4 \left\| \theta^{(i)} \right\|_{\infty} + 2 \right) \geq \lambda > 0. \end{split}$$

As for $1 \le k \le m-1$, we have the following estimate:

(3.9)

$$\begin{split} w_{k+1} \left(\theta_{j}^{n,(3)} + \sigma_{j-1}^{n} \right) + w_{k} \left(\theta_{j}^{n,(4)} - \theta_{j}^{n,(3)} + \sigma_{j}^{n} \right) - w_{k-1} \left(\theta_{j}^{n,(4)} + \sigma_{j+1}^{n} \right) \\ &= w_{k+1} \theta_{j+1}^{n,(3)} + w_{k} \left(\theta_{j+1}^{n,(4)} - \theta_{j+1}^{n,(3)} \right) - w_{k-1} \theta_{j+1}^{n,(4)} - w_{k+1} \left(\gamma_{13} r_{j}^{n} + \gamma_{23} r_{j+1}^{n} \right) \\ &- w_{k} \left((\gamma_{13} + \gamma_{14}) r_{j}^{n} + (\gamma_{23} + \gamma_{24}) r_{j+1}^{n} \right) - w_{k-1} \left(\gamma_{14} r_{j}^{n} + \gamma_{24} r_{j+1}^{n} \right) \\ &= \left(w_{k+1} - w_{k} \right) \theta_{j+1}^{n,(3)} + \left(w_{k} - w_{k-1} \right) \theta_{j+1}^{n,(4)} - \left(\gamma_{13} (w_{k} + w_{k+1}) + \gamma_{14} (w_{k-1} + w_{k}) \right) r_{j}^{n} \\ &- \left(\gamma_{23} (w_{k} + w_{k+1}) + \gamma_{24} (w_{k-1} + w_{k}) \right) r_{j+1}^{n} \ge c \left(\frac{h}{\delta} \right)^{2} \rho_{\min} - 2 \frac{h}{\delta} w(0) L h \ge 0. \end{split}$$

Note that in the last two steps of the estimate (3.9), the inductive hypothesis $r_j^n \ge -Lh$ for $j \in \mathbb{Z}$ is used, along with the condition $0 < \delta \le \delta_0$ as specified in (2.28) and the following facts:

$$\begin{aligned} &\theta_{j+1}^{n,(3)} + \theta_{j+1}^{n,(4)} \leq -\rho_{\min}; \quad \gamma_{13} + \gamma_{23} + \gamma_{14} + \gamma_{24} = -1; \\ &w_k - w_{k+1} \geq c \left(\frac{h}{\delta}\right)^2, \quad w_k + w_{k+1} \leq 2\frac{h}{\delta}w(0), \quad k = 0, \dots, m-1. \end{aligned}$$

We then immediately get $c_{j,k}^n \ge 0$ for $2 \le k \le m-1$. Furthermore, $c_{j,1}^n \ge 0$ follows from (3.9) together with the inequality

$$-\theta_j^{n,(2)} + 2(\gamma_{23} + \gamma_{24})r_{j+1}^n \ge -\theta_j^{n,(2)} + 2(\gamma_{23} + \gamma_{24}) \ge 0.$$

Finally, $\theta_j^{n,(4)} + \sigma_{j+1}^n = \theta_{j+2}^{n,(4)} \leq 0$ leads to $c_{j,m}^n \geq 0$. Therefore, r_j^{n+1} is a convex combination of $\{r_{j+k}^n\}_{k=-1}^m$ plus the two nonnegative terms given in (3.8). Consequently, if the estimate $r_j^n \geq -Lh \ \forall j \in \mathbb{Z}$ holds for any $n \geq 0$, it implies that the estimate also holds for n+1. Thus, by induction, the claim is proved, and with that, (3.4) is established. This completes the proof.

Based on Lemma 2, a more careful analysis gives the following sharper estimate corresponding to the entropy condition (2.5).

Lemma 3. Suppose all conditions in Theorem 1 are met and $0 < h \le \frac{1}{4L}$. We have

(3.10)
$$L^{n} \leq \frac{1}{\frac{1}{L^{0}} + 2n\tau} \leq \frac{1}{2n\tau}, \quad n \geq 1,$$

where $L^n \doteq \sup_{j \in \mathbb{Z}} \max \{-r_j^n/h, 0\}$ for $n \geq 0$ and r_j^n is as in Lemma 2.

Proof. We still start with (3.8). For $k \neq 0, 1$, we use the estimate

(3.11)
$$c_{j,k}^{n}r_{j+k}^{n} \ge -c_{j,k}^{n}L^{n}h.$$

In the case of k = 0 and k = 1, we consider the quadratic polynomials

$$b_0(r_i^n) \doteq c_{i,0}^n r_i^n - 2\lambda(\gamma_{13} + \gamma_{14})(r_i^n)^2, \quad b_1(r_{i+1}^n) \doteq c_{i,1}^n r_{i+1}^n - 2\lambda(\gamma_{23} + \gamma_{24})(r_{i+1}^n)^2,$$

and leverage the estimates

$$c_{j,0}^{n} \ge \lambda$$
, $c_{j,1}^{n} \ge \lambda \left(-\theta_{j}^{n,(2)} + 2(\gamma_{23} + \gamma_{24})r_{j+1}^{n} \right)$

which have been used in the proof of Lemma 2. This leads to

$$b_0'(r_i^n) = c_{i,0}^n - 4\lambda(\gamma_{13} + \gamma_{14})r_i^n \ge \lambda - 4\lambda Lh \ge 0,$$

when $h \leq \frac{1}{4L}$, and

$$b_1'(r_{j+1}^n) = c_{j,1}^n - 4\lambda(\gamma_{23} + \gamma_{24})r_{j+1}^n \ge \lambda\left(-\theta_j^{n,(2)} + 2(\gamma_{23} + \gamma_{24})\right) \ge 0.$$

Therefore we have

(3.12)
$$b_0(r_j^n) \ge -c_{j,0}^n L^n h - 2\lambda (\gamma_{13} + \gamma_{14}) (L^n h)^2,$$
$$b_1(r_{j+1}^n) \ge -c_{j,1}^n L^n h - 2\lambda (\gamma_{23} + \gamma_{24}) (L^n h)^2.$$

By summing (3.11) for $k \neq 0, 1$ and (3.12) for k = 0, 1, and noting that $\gamma_{13} + \gamma_{14} + \gamma_{23} + \gamma_{24} = -1$, we obtain

$$r_i^{n+1} \ge -L^n h + 2\lambda (L^n h)^2 = -L^n h + 2(L^n)^2 h \tau$$

which further yields $L^{n+1} \leq L^n - 2(L^n)^2 \tau$. This completes the proof by induction, as (3.10) follows through the following calculation:

$$\frac{1}{L^{n+1}} - \frac{1}{L^n} = \frac{L^n - L^{n+1}}{L^n L^{n+1}} \ge \frac{2(L^n)^2 \tau}{L^n L^{n+1}} \ge 2\tau.$$

With the one-sided Lipschitz estimate (3.4) in hand, we are now ready to revisit the monotonicity verification of the scheme (2.16)–(2.17).

LEMMA 4. Suppose all conditions in Theorem 1 are met. The scheme (2.16)-(2.17) is monotone, meaning that the function \mathcal{H} defined in (2.16)–(2.17) is nondecreasing with respect to each of its arguments.

Proof. We employ (3.2) along with the notations and estimates in Lemma 2. The proof offered here closely parallels the one for Lemma 2.

For k = -1 and k = 0, we have the following estimate:

$$\frac{\partial \mathcal{H}}{\partial \rho_{j-1}^{n}} \ge \lambda \left(\theta_{j}^{n,(1)} + \theta_{j}^{n,(3)} \right) \ge 0,$$

$$\frac{\partial \mathcal{H}}{\partial \rho_{j}^{n}} \ge 1 - \lambda \left(\sum_{i=1}^{4} \left\| \theta^{(i)} \right\|_{\infty} - (\gamma_{13} + \gamma_{23}) \right) \ge 1 - \lambda \left(\sum_{i=1}^{4} \left\| \theta^{(i)} \right\|_{\infty} + 1 \right) \ge 0.$$

For k=m, we have $\frac{\partial \mathcal{H}}{\partial \rho_{j+m}^n} = -\lambda w_{m-1} \theta_{j+1}^{n,(4)} \geq 0$. For $k=1,\ldots,m-1$, we utilize the following estimate, similar to the derivation of (3.9):

$$\begin{split} w_{k+1}\theta_{j}^{n,(3)} - w_{k}\theta_{j+1}^{n,(3)} + w_{k}\theta_{j}^{n,(4)} - w_{k-1}\theta_{j+1}^{n,(4)} \\ &= (w_{k+1} - w_{k})\theta_{j}^{n,(3)} + (w_{k} - w_{k-1})\theta_{j}^{n,(4)} - (\gamma_{13}w_{k} + \gamma_{14}w_{k-1})r_{j-1}^{n} \\ &- (\gamma_{23}w_{k} + \gamma_{24}w_{k-1})r_{j}^{n} \\ &\geq c\left(\frac{h}{\delta}\right)^{2}\rho_{\min} - 2\frac{h}{\delta}w(0)Lh \geq 0, \end{split}$$

with the last inequality being implied again by (2.28). The above estimate implies $\frac{\partial \mathcal{H}}{\partial \rho_{j+k}^n} \geq 0$ for $k=2,\ldots,m-1$. Moreover, $\frac{\partial \mathcal{H}}{\partial \rho_{j+1}^n} \geq 0$ follows from the above estimate and $-\theta_{j+1}^{n,(2)} \ge 0$.

An immediate consequence of the monotonicity of the scheme is its TVD property, as established in the following Lemma 5. The proof of the lemma is similar to that in [32] for monotone schemes of scalar conservation laws.

Lemma 5. Suppose all conditions in Theorem 1 are met. The numerical solution $\{\rho_i^n\}_{i\in\mathbb{Z}}^{n\geq 0}$ produced by the scheme (2.16)–(2.17) satisfies

$$\sum_{j \in \mathbb{Z}} |\rho_{j+1}^n - \rho_j^n| \le \sum_{j \in \mathbb{Z}} |\rho_{j+1}^0 - \rho_j^0| \le \mathrm{TV}(\rho_0) \quad \forall n \ge 0.$$

Putting all of the results in the last two sections together, the proof of Theorem 1 is now complete.

3.3. Convergence. In this subsection, we are going to give the proofs of Theorem 2 and Theorem 3. The given proofs are similar to those in the existing literature such as [7, 22]; here we only provide the key ingredients of the proofs.

Proof of Theorem 2. We recall that the numerical solution $\rho^{\delta,h}$ is defined as

(3.13)
$$\rho^{\delta,h}(t,x) = \sum_{j \in \mathbb{Z}} \sum_{n=0}^{\infty} \rho_j^n \mathbf{1}_{\mathcal{C}_j \times \mathcal{T}^n}(t,x),$$

where $C_j = (x_{j-1/2}, x_{j+1/2})$ and $T^n = (t^n, t^{n+1})$. For any test function $\phi \in \mathbf{C}^1_{\mathbf{c}}([0, +\infty)]$ $\times \mathbb{R}$), we denote $\phi_i^n = \phi(t^n, x_j)$ for all $j \in \mathbb{Z}$ and $n \ge 0$.

Let us consider the family of numerical solutions $\{\rho^{\delta,h}\}_{0<\delta\leq\delta_0,0< h<1}$, where δ_0 is as in (2.28). The maximum principle (2.2) gives the a priori \mathbf{L}^{∞} estimate for $\rho^{\delta,h}$. Moreover, Lemma 5 gives the spatial total variation bound on $\rho^{\delta,h}$, and consequently the temporal total variation bound is given by

$$\sum_{j \in \mathbb{Z}} |\rho_j^{n+1} - \rho_j^n| \le \lambda \left(\sum_{i=1}^4 \left\| \theta^{(i)} \right\|_{\infty} \right) \sum_{j \in \mathbb{Z}} |\rho_{j+1}^n - \rho_j^n| \le \mathrm{TV}(\rho_0) \quad \forall n \ge 0.$$

Therefore, the family of numerical solutions is uniformly bounded in $\mathbf{BV}_{loc}([0,+\infty) \times \mathbb{R})$. Thus, it is precompact in the \mathbf{L}^1_{loc} norm (see [23]), and there exists a sequence $\{\rho^{\delta_l,h_l}\}$ converging in $\mathbf{L}^1_{loc}([0,+\infty) \times \mathbb{R})$ to a limit function ρ^* as $\delta_l \to 0, h_l \to 0$ simultaneously. Noting the uniqueness of the entropy solution, to show the convergence of $\rho^{\delta,h}$ when $\delta \to 0$ and $h \to 0$ along an arbitrary path, we only need to show that ρ^* satisfies both the weak form (2.4) and the entropy condition (2.5).

For the weak form (2.4), we begin by multiplying the scheme (2.16)–(2.17) by $\phi_j^n h$, summing over all $j \in \mathbb{Z}$ and $n \ge 0$, and then applying summation by parts. This leads us to

(3.14)

$$h\tau \sum_{n\geq 1} \sum_{j\in\mathbb{Z}} \frac{\phi_j^n - \phi_j^{n-1}}{\tau} \rho_j^n + h\tau \sum_{n\geq 0} \sum_{j\in\mathbb{Z}} \frac{\phi_{j+1}^n - \phi_j^n}{h} g(\rho_j^n, \rho_{j+1}^n, q_j^n, q_{j+1}^n) + h \sum_{j\in\mathbb{Z}} \phi_j^0 \rho_j^0 = 0.$$

Then we take the limit as $\delta \to 0$ and $h \to 0$ simultaneously on both sides of (3.14), while utilizing the following key estimates:

(3.15)

$$\begin{split} h \sum_{j \in \mathbb{Z}} |g(\rho_j^n, \rho_{j+1}^n, q_j^n, q_{j+1}^n) - \rho_j v(q_j^n)| \\ &= h \sum_{j \in \mathbb{Z}} |g(\rho_j^n, \rho_{j+1}^n, q_j^n, q_{j+1}^n) - g(\rho_j^n, \rho_j^n, q_j^n, q_j^n)| \le 2 \left(\sum_{i=1}^4 \left\| \theta^{(i)} \right\|_{\infty} \right) \text{TV}(\rho_0) h, \end{split}$$

and

$$h \sum_{j \in \mathbb{Z}} |\rho_j v(q_j^n) - \rho_j v(\rho_j^n)| \le h \sum_{j \in \mathbb{Z}} |q_j^n - \rho_j^n| \le h \left(\sum_{k=1}^{m-1} k w_k\right) \sum_{j \in \mathbb{Z}} |\rho_{j+1}^n - \rho_j^n|$$

$$\le \frac{1}{2} w(0) \text{TV}(\rho_0) \delta,$$

which implies (2.4).

For the entropy condition, let us consider numerical solutions $\tilde{\rho}^{\delta,h}$ that are constructed by linear interpolation rather than the piecewise constant reconstruction as defined in (3.13). Then by Lemma 3, $\tilde{\rho}^{\delta,h}$ satisfies the one-sided Lipschitz estimate:

$$(3.16) -\frac{\tilde{\rho}^{\delta,h}(t,y) - \tilde{\rho}^{\delta,h}(t,x)}{y-x} \le \frac{1}{2t} \quad \forall x \ne y \in \mathbb{R}, t > 0.$$

Noting that $\tilde{\rho}^{\delta,h}$ converges to the same limit function ρ^* pointwise, we can show that ρ^* satisfies the Oleinik entropy condition (2.5) by passing the limit on (3.16).

To prove Theorem 3, we first prove the following lemma.

LEMMA 6. Take Assumptions 1–5 and that δ satisfies the condition (2.28). When $\delta \to \delta_* > 0$ and $h \to 0$, the numerical solution $\rho^{\delta,h}$ produced by the scheme (2.16)–(2.17) converges in $\mathbf{L}^1_{loc}([0,+\infty)\times\mathbb{R})$ to the weak solution ρ^{δ_*} of the nonlocal LWR model (1.2) as defined in Proposition 1.

Proof. Similarly as in the proof of Theorem 2, when taking the limit $\delta \to \delta_*$ and $h \to 0$, there exists a sequence $\{\rho^{\delta_l,h_l}\}$ converging to a limit function ρ^{**} in the $\mathbf{L}^1_{\mathrm{loc}}$ norm with $\delta_l \to \delta_*, h_l \to 0$. Noting that Proposition 1 already gives the solution uniqueness, we only need to show that the limit function ρ^{**} satisfies the weak form (2.1).

The weak form (2.1) can be obtained by taking the limit $\delta_l \to \delta_*, h_l \to 0$ on both sides of (3.14) and utilizing the estimate (3.15) as well as the convergence

(3.17)
$$\sum_{j\in\mathbb{Z}}\sum_{n=0}^{\infty}q_{j}^{n}\mathbf{1}_{\mathcal{C}_{j}\times\mathcal{T}^{n}}(t,x)\to\int_{0}^{\delta}\rho^{\delta,h}(t,x+s)w_{\delta}(s)\,ds$$

in the $\mathbf{L}_{\mathrm{loc}}^1$ norm.

We now give the proof of Theorem 3.

Proof of Theorem 3. For a bounded domain $U \subset [0, +\infty) \times \mathbb{R}$, suppose (2.30) is not true, and there exists a sequence of δ_l and h_l where $\delta_l \in (0, \delta_0]$ and $h_l \to 0$ as $l \to \infty$, and $\varepsilon > 0$, such that

$$\|\rho^{\delta_l,h_l}-\rho^{\delta_l}\|_{\mathbf{L}^1(U)}\geq \varepsilon.$$

By possibly selecting a subsequence we suppose $\delta_l \to \delta_* \in [0, \delta_0]$. If $\delta_l \to 0$, both ρ^{δ_l, h_l} and ρ^{δ_l} converge to ρ^0 ; if $\delta_l \to \delta_* > 0$, by Lemma 6, $\rho^{\delta_l, h_l} \to \rho^{\delta_*}$, and by applying the same arguments on continuous solutions, it holds that $\rho^{\delta_l} \to \rho^{\delta_*}$. In both cases there is a contradiction.

3.4. Local limit of numerical discretizations. We now present the proof of Theorem 4.

Proof of Theorem 4. We first prove (2.31). By the Assumption 3, the numerical solution satisfies $q_j^n = \rho_j^n$ for all $j \in \mathbb{Z}$ and $n \ge 0$ whenever $0 < \delta < h$. This implies that the two schemes (2.16)–(2.17) and (2.18) are exactly the same, and thus (2.31) holds.

Next we prove (2.32). For a bounded domain $U \subset [0, +\infty) \times \mathbb{R}$, suppose (2.32) is not true, and there exists a sequence of δ_l and h_l where $0 < h_l \le \delta_l \to 0$ as $l \to \infty$, and $\varepsilon > 0$, such that

$$\|\rho^{\delta_l,h_l}-\rho^{0,h_l}\|_{\mathbf{L}^1(U)}\geq \varepsilon.$$

But this contradicts the fact that both ρ^{δ_l,h_l} and ρ^{0,h_l} converge to ρ^0 as $l \to \infty$.

4. Numerical experiments. In this section, we test the presented numerical scheme (2.16)–(2.17) in several numerical experiments to demonstrate the established results. In these numerical experiments, we choose the numerical quadrature weights $\{w_k\}_{k=0}^{m-1}$ from the ones given in (2.12), (2.33), and (2.14) and fix the CFL ratio $\lambda = 0.25$. In all but the fourth experiment, we use the linear decreasing kernel $w_{\delta}(s) = \frac{2}{\delta^2}(\delta - s)$. Assuming $\delta = mh$, where m is a positive integer, the numerical quadrature weights for the linear decreasing kernel computed from (2.12), (2.33), and (2.14) are given, respectively, by the following:

- $\begin{array}{l} \bullet \ \ \text{(Left endpoint)} \ w_k = \frac{2(m-k)}{m^2} \ \text{for} \ 0 \leq k \leq m-1, \ \text{with} \ \sum_{k=0}^{m-1} w_k = 1 + \frac{1}{m}; \\ \bullet \ \ \text{(Normalized left endpoint)} \ w_k = \frac{2(m-k)}{m(m+1)} \ \text{for} \ 0 \leq k \leq m-1, \ \text{with} \ \sum_{k=0}^{m-1} w_k = 1; \\ \bullet \ \ \text{(Exact quadrature)} \ w_k = \frac{2(m-k)-1}{m^2} \ \text{for} \ 0 \leq k \leq m-1, \ \text{with} \ \sum_{k=0}^{m-1} w_k = 1. \\ \text{In all but the fifth experiment, the velocity function is chosen to be} \ v(\rho) = 1 \rho. \end{array}$

Two sets of initial data ρ_0 are used; one is a bell-shaped curve,

(4.1)
$$\rho_0(x) = 0.4 + 0.4 \exp\left(-100(x - 0.5)^2\right), \quad x \in \mathbb{R},$$

while the other represents the Riemann data:

(4.2)
$$\rho_0(x) = \begin{cases} \rho_L, & x < 0.5, \\ \rho_R, & x > 0.5, \end{cases} \quad x \in \mathbb{R};$$

we take $\rho_L = 0.1$ and $\rho_R = 0.6$ in all the experiments. The numerical solutions are presented on the spatial domain $x \in [0,1]$ and in the time horizon $t \in [0,1]$ even though the numerical computations are done on a larger spatial domain with the constant extension on both sides. In the first three experiments, we examine the asymptotic compatibility of the scheme (2.16)–(2.17) with different numerical quadrature weights. In the fourth experiment, we test the scheme with different choices of the nonlocal kernel. In the fifth experiment, we test the scheme with nonlinear velocity functions $v = v(\rho)$ other than the linear one $v(\rho) = 1 - \rho$.

Experiment 1. We first present numerical solutions $\rho^{\delta,h}$ computed with the Lax-Friedrichs numerical flux function (2.27a) and different numerical quadrature weights. For each initial data and each set of numerical quadrature weights, we compute the numerical solution $\rho^{\delta,h}$ with $\delta = 0.005, h = 0.001$ and plot its snapshots at selected times t = 0, 0.5, 1. Moreover, the snapshot of the numerical solution $\rho^{\delta,h}$ at time t=1 is compared with that of the solution ρ^0 of the local model (1.1). In this experiment, the local solution ρ^0 is also computed numerically because the analytical solution is not always available. The numerical computation is done on a fine grid with h = 0.0002 using a Lax-Friedrichs scheme for (1.1) with the numerical flux function

$$(4.3) g_{\text{local}}(\rho_L, \rho_R) = \frac{1}{2}(\rho_L v(\rho_L) + \rho_R v(\rho_R)) + \frac{\alpha}{2}(\rho_L - \rho_R),$$

which is the local counterpart of (2.27a). The snapshot of the local solution ρ^0 at time t=1 is plotted with dashed line. See Figure 4.1.

For the bell-shaped initial data, we observe from the top row of Figure 4.1 that the numerical solutions of the nonlocal model preserve the smoothness of the initial data while the local solution develops a shock. At time t=1, the numerical solutions of the nonlocal model computed with the normalized left endpoint quadrature weights and the exact quadrature weights are close to the local solution, especially in the region away from the shock of the local solution. This means that the numerical solution $\rho^{\delta,h}$ with both δ,h small provides a good approximation to the local solution ρ^0 , which validates the conclusion of Theorem 2. We also observe from the top left figure of Figure 4.1 that the numerical solution of the nonlocal model computed with the left endpoint quadrature weights is very different from the local solution at time t=1. Although the numerical solution of the nonlocal model still approximates a shock profile at time t=1, the shock position is incorrect. The comparison between the three sets of numerical quadrature weights emphasizes the significance of the normalization condition (2.20) for numerical quadrature weights.

For the Riemann initial data, the local solution ρ^0 is a traveling wave moving at the constant speed $v = 1 - (\rho_L + \rho_R) = 0.3$. We observe from the bottom row

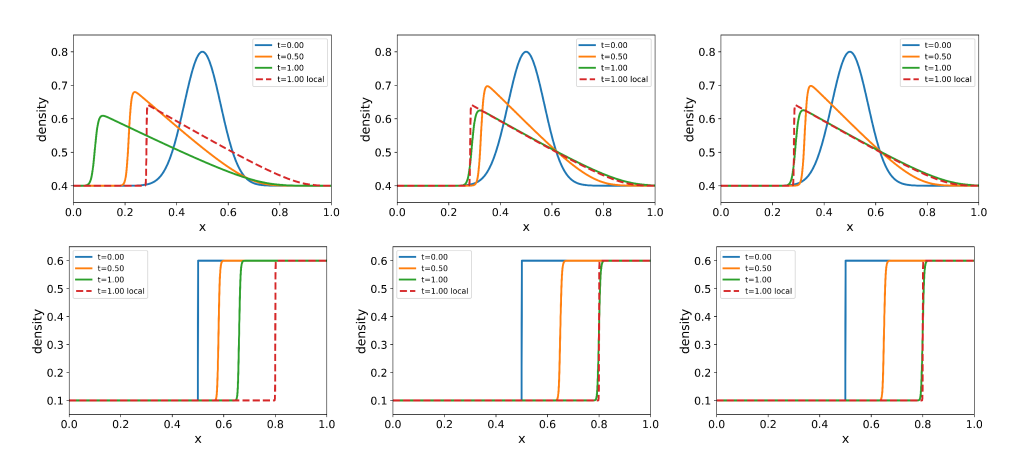


FIG. 4.1. Experiment 1: Snapshots of computed solutions for the bell-shaped initial data (top) and the Riemann initial data (bottom) corresponding to the left endpoint quadrature weights (left), the normalized left endpoint quadrature weights (middle), and the exact quadrature weights (right).

of Figure 4.1 that the numerical solutions of the nonlocal model computed with the normalized left endpoint quadrature weights and the exact quadrature weights are close to the local solution at time t=1 while the nonlocal solutions get smoothed because of the nonlocal effects, but the one computed with the left endpoint quadrature weights indicates an incorrect position for the jump from $\rho_L = 0.1$ to $\rho_R = 0.6$.

Experiment 2. We next check the asymptotic compatibility of the scheme (2.16)-(2.17) by plotting $\|\rho^{\delta,h}-\rho^0\|_{\mathbf{L}^1}$ with $\delta\propto h\to 0$. We take $\delta=mh$, where m=1,2,5 and $h=0.01\times 2^{-l}$ for l=0,1,2,3, and compute numerical solutions $\rho^{\delta,h}$ using the Lax-Friedrichs numerical flux function (2.27a) and different numerical quadrature weights. The local solution ρ^0 is numerically solved on a fine grid with $h=0.01\times 2^{-5}$ using a Lax-Friedrichs scheme for (1.1) with the numerical flux function (4.3). For each initial data and each set of numerical quadrature weights, we compute the \mathbf{L}^1 error $\|\rho^{\delta,h}-\rho^0\|_{\mathbf{L}^1}$ with an interpolation of $\rho^{\delta,h}$ onto the fine grid on which ρ^0 is computed and plot $\|\rho^{\delta,h}-\rho^0\|_{\mathbf{L}^1}$ against h^{-1} in the log-log scale for $\delta=h$, $\delta=2h$, and $\delta=5h$ in different colors. In this approach, both δ and h decrease to zero, keeping the ratio $m=\delta/h$ constant. By doing so, each plotted line showcases the convergence from $\rho^{\delta,h}$ to ρ^0 along the specific limiting path defined by $\delta=mh\to 0$. We also plot a dashed line with the slope -1 to represent the linear convergence rate. See the results in Figure 4.2.

We observe from Figure 4.2 that, for the normalized left endpoint quadrature weights and the exact quadrature weights, the error $\|\rho^{\delta,h} - \rho^0\|_{\mathbf{L}^1}$ has a linear decay rate with respect to h for both initial data and $\delta = mh$ for m = 1, 2, 5. This means that $\rho^{\delta,h}$ converges to ρ^0 along the limiting paths $\delta = mh \to 0$ for m = 1, 2, 5, which validates the conclusion of Theorem 2. Moreover, the numerical results show that the convergence is of first order with the particular choices of the initial data and the limiting paths. In contrast, for the left endpoint numerical quadrature weights, the error $\|\rho^{\delta,h} - \rho^0\|_{\mathbf{L}^1}$ stagnates on the scale of 10^{-1} for both initial data and $\delta = mh$ for m = 1, 2, 5. This is due to the convergence of $\rho^{\delta,h}$ to an incorrect solution when $\delta = mh \to 0$.

Experiment 3. We now check the asymptotic compatibility of the scheme (2.16)–(2.17) by plotting $\|\rho^{\delta,h}-\rho^{\delta}\|_{\mathbf{L}^1}$ with $h\to 0$ for different choices of δ . We

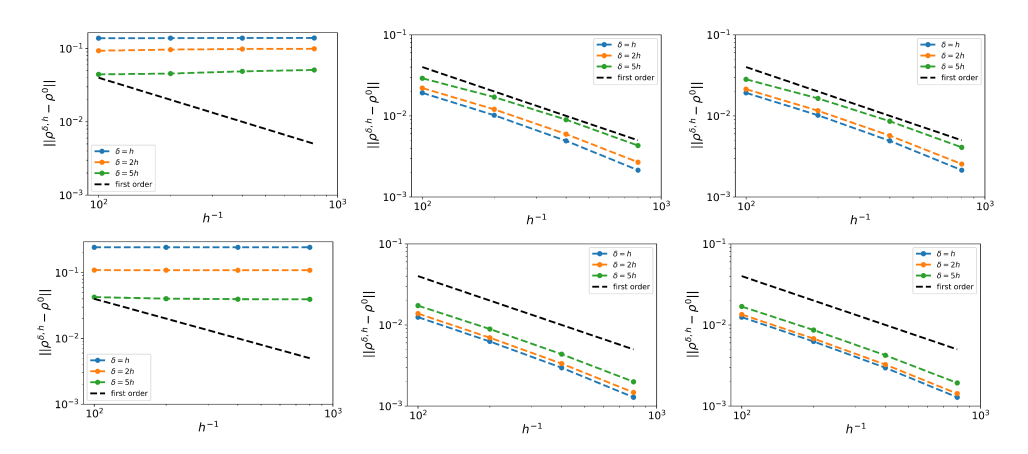


Fig. 4.2. Experiment 2: Convergence from $\rho^{\delta,h}$ to ρ^0 for the bell-shaped initial data (top) and the Riemann initial data (bottom) corresponding to the left endpoint quadrature weights (left), the normalized left endpoint quadrature weights (middle), and the exact quadrature weights (right).

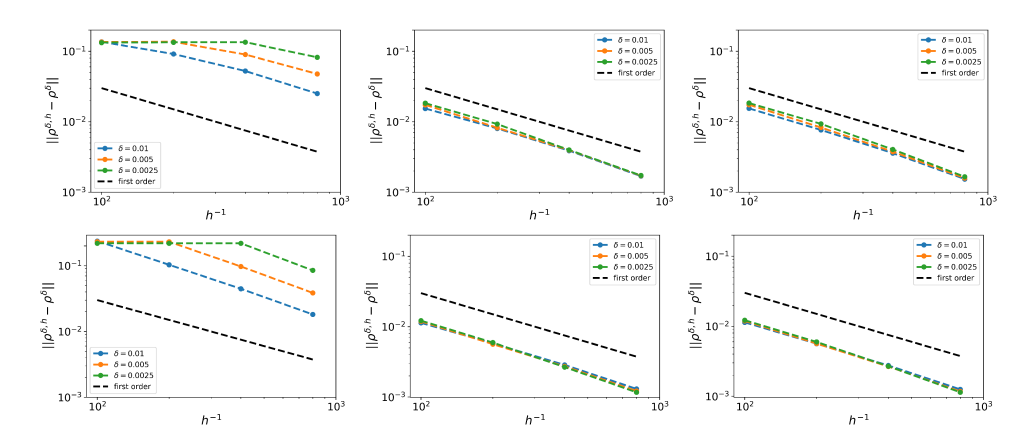


FIG. 4.3. Experiment 3: Convergence from $\rho^{\delta,h}$ to ρ^{δ} for the bell-shaped initial data (top) and the Riemann initial data (bottom) corresponding to the left endpoint quadrature weights (left), the normalized left endpoint quadrature weights (middle), and the exact quadrature weights (right).

take $\delta = 0.01 \times 2^{-l}$ for l = 0, 1, 2 and $h = 0.01 \times 2^{-l}$ for l = 0, 1, 2, 3, and we compute numerical solutions $\rho^{\delta,h}$ using the Lax–Friedrichs numerical flux function (2.27a) and different numerical quadrature weights. The reference solution ρ^{δ} is numerically solved on a fine grid with $h = 0.01 \times 2^{-5}$ using the same scheme. For each initial data and each set of numerical quadrature weights, we compute the \mathbf{L}^1 error $\|\rho^{\delta,h} - \rho^{\delta}\|_{\mathbf{L}^1}$ with an interpolation of $\rho^{\delta,h}$ onto the fine grid, and plot $\|\rho^{\delta,h} - \rho^{\delta}\|_{\mathbf{L}^1}$ with respect to h^{-1} in the log-log scale for $\delta = 0.01$, $\delta = 0.005$, and $\delta = 0.0025$ in different colors. A dashed line with the slope -1 is again provided. See the results in Figure 4.3.

From Figure 4.3, we see that for the normalized left endpoint quadrature weights and the exact quadrature weights, the error $\|\rho^{\delta,h} - \rho^{\delta}\|_{\mathbf{L}^1}$ has a linear decay rate with respect to h for both initial data and all choices of δ . Moreover, the plots of $\|\rho^{\delta,h} - \rho^{\delta}\|_{\mathbf{L}^1}$ with respect to h^{-1} have very little change for $\delta = 0.01$, $\delta = 0.005$, and $\delta = 0.0025$. This means that $\rho^{\delta,h}$ converges to ρ^{δ} as $h \to 0$ uniformly in δ , which validates the conclusion of Theorem 3. In addition, the numerical results show that

the convergence is of first order with the particular choices of the initial data and the parameter δ . In contrast, for the left endpoint numerical quadrature weights, the error $\|\rho^{\delta,h} - \rho^{\delta}\|_{\mathbf{L}^1}$ stagnates on the scale of 10^{-1} when $h \geq \delta$ for both initial data and all choices of δ . This may because ρ^{δ} approximates ρ^{0} well when δ is small while $\rho^{\delta,h} = \rho^{0,h}$ when $h \geq \delta$ and $\rho^{0,h}$ is not a consistent numerical approximation to ρ^{0} . We also observe that, in each case, the error decays when $h < \delta$. However, the error increases when δ decreases from 0.01 to 0.0025 for any fixed mesh size h. One can infer that the convergence from $\rho^{\delta,h}$ to ρ^{δ} as $h \to 0$ will become slower and slower as $\delta \to 0$, and the uniform convergence cannot hold, which is again showing the importance of the normalization condition (2.20) for the uniform convergence of the scheme (2.16)–(2.17).

Experiment 4. In this experiment we test the scheme (2.16)–(2.17) with different choices of the nonlocal kernel. Besides the linear decreasing kernel considered before, we also use the exponential kernel $w_{\delta}(s) = \frac{e^{-\frac{s}{\delta}}}{\delta(1-e^{-1})}$ and the constant kernel $w_{\delta}(s) = \frac{1}{\delta}$ and adopt the exact quadrature weights (2.14). We take $\delta = mh$, where m = 1, 2, 5, and $h = 0.01 \times 2^{-l}$ for l = 0, 1, 2, 3, and we compute numerical solutions $\rho^{\delta,h}$ using the Lax–Friedrichs numerical flux function (2.27a) and different numerical quadrature weights. The local solution ρ^0 is numerically solved on a fine grid with $h = 0.01 \times 2^{-5}$ using a Lax–Friedrichs scheme for (1.1) with the numerical flux function (4.3). For each initial data and each nonlocal kernel, we compute the \mathbf{L}^1 error $\|\rho^{\delta,h}-\rho^0\|_{\mathbf{L}^1}$. A dashed line with the slope -1 is again provided. See the results in Figure 4.4.

We observe from Figure 4.4 that, for all the three nonlocal kernels, the error $\|\rho^{\delta,h}-\rho^0\|_{\mathbf{L}^1}$ has a linear decay rate with respect to h for both initial data and in all cases $\delta=mh$ for m=1,2,5. Moreover, the plots for the three nonlocal kernels have little difference. For the linear decreasing kernel and the exponential kernel, the convergence result validates the conclusion of Theorem 2. For the constant kernel, it does not satisfy the condition that $w=w_{\delta}(s)$ is strictly decreasing, and (2.19) does not hold because $w_{k-1}-w_k=0$ for all $k=1,\ldots,m-1$. In this case, the analysis used in the proof of Theorem 1 cannot give the necessary estimates on numerical solutions, but the numerical results show that the conclusion of Theorem 2 may still be true.

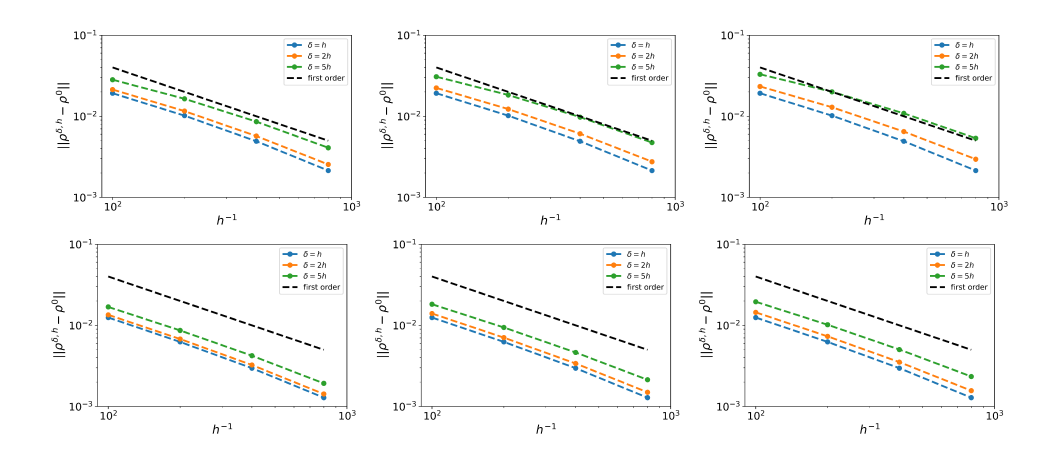


FIG. 4.4. Experiment 4: Convergence from $\rho^{\delta,h}$ to ρ^0 for the bell-shaped initial data (top) and the Riemann initial data (bottom) corresponding to the linear decreasing kernel (left), the exponential kernel (middle), and the constant kernel (right).

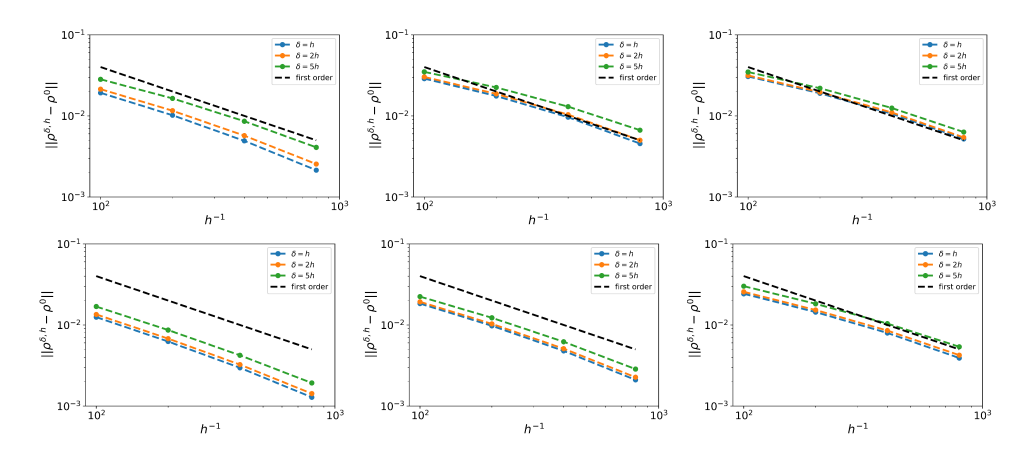


FIG. 4.5. Experiment 5: Convergence from $\rho^{\delta,h}$ to ρ^0 for the bell-shaped initial data (top) and the Riemann initial data (bottom) corresponding to the linear velocity function $v(\rho) = 1 - \rho$ (left), the Underwood velocity function $v(\rho) = e^{-\rho}$ (middle), and the Krystek velocity function $v(\rho) = (1 - \rho)^4$ (right).

Experiment 5. In this experiment, we evaluate the scheme (2.16)–(2.17) with nonlinear velocity functions other than the linear one $v(\rho) = 1 - \rho$. We take the following nonlinear velocity functions that have been employed in traffic flow modeling [40, 53] (for a comprehensive review of other velocity functions, see [46]):

[Underwood]
$$v(\rho) = e^{-\rho}$$
,
[Krystek] $v(\rho) = (1 - \rho)^4$.

The nonlocal velocity is determined using (1.3). Within this, we use the linear decreasing kernel $w_{\delta}(s) = \frac{2}{\delta^2}(\delta - s)$ and adopt the exact quadrature weights (2.14).

Similar to Experiment 4, we choose $\delta = mh$ with m = 1, 2, 5 and $h = 0.01 \times 2^{-l}$ for l = 0, 1, 2, 3. The numerical solutions $\rho^{\delta,h}$ are computed using the Lax–Friedrichs-type numerical flux function (2.27a). The local solution ρ^0 is numerically solved on a fine grid with $h = 0.01 \times 2^{-5}$ using a Lax–Friedrichs scheme for (1.1) accompanied by the numerical flux function (4.3). For each initial data and each velocity function, we compute the \mathbf{L}^1 error $\|\rho^{\delta,h} - \rho^0\|_{\mathbf{L}^1}$. A reference dashed line with the slope -1 is provided as in previous experiments. See the results in Figure 4.5.

We observe from Figure 4.5 that, for both of the tested nonlinear velocity functions, the error $\|\rho^{\delta,h}-\rho^0\|_{\mathbf{L}^1}$ has a linear decay rate with respect to h for both initial data and in all cases $\delta=mh$ for m=1,2,5. This is consistent with the linear velocity function. Moreover, although there are slight variations among the plots for the three velocity functions, the linear velocity function yields the smallest absolute error $\|\rho^{\delta,h}-\rho^0\|_{\mathbf{L}^1}$ when given the same parameters δ and h. These numerical findings suggest that Theorem 2 might be applicable to nonlinear velocity functions, provided that its assumption on the numerical flux function is suitably modified.

5. Conclusions and future work. In this work, finite volume numerical schemes (2.16)–(2.17) are studied for solving the nonlocal LWR model (1.2) with a parameter δ that measures the range of information exchange. An important observation is that, based on both numerical analysis and computational experiments, certain numerical quadrature weights that provide consistent approximations in the case of a given $\delta > 0$ may lead to consistency between the scheme (2.16)–(2.17) and the local limit (1.1)

of the nonlocal model (1.2) as $\delta \to 0$ and $h \to 0$. For properly selected numerical quadrature weights, we are able to prove, under reasonable assumptions, that the numerical solutions of the nonlocal model converge to the continuous solution of the nonlocal model with a fixed $\delta > 0$ as $h \to 0$, while they converge to the entropy solution of the local continuum model (1.1) as $\delta \to 0$ and $h \to 0$ simultaneously. That is, such schemes are asymptotically compatible with its local limit. We are able to demonstrate that these asymptotically compatible schemes can offer robust numerical simulations under the changes in δ due to the uniform convergence when the values of δ are within a proper range.

Our established results are based on the a priori estimates on the numerical solutions as given in Theorem 1, subject to assumptions alluded to above. As shown in the computational experiments, the normalization condition for numerical quadrature weights is essential to the asymptotic compatibility of the scheme (2.16)–(2.17). The experiments also suggest that the results of this work may be extended to the cases with more general nonlocal kernels and velocity functions $v = v(\rho)$ other than the linear one $v(\rho) = 1 - \rho$. It might also be possible to establish the results with more general initial data that may have negative jumps. Furthermore, with the a priori bounds on the numerical solutions and known estimates on the exact solutions, it is possible to derive a priori error estimates subject to suitable conditions on the regularities of continuous solutions. These questions along with further generalizations and applications of nonlocal traffic flow models will be subjects of future research.

REFERENCES

- A. AGGARWAL, R. M. COLOMBO, AND P. GOATIN, Nonlocal systems of conservation laws in several space dimensions, SIAM J. Numer. Anal., 53 (2015), pp. 963–983.
- [2] A. AGGARWAL, H. HOLDEN, AND G. VAIDYA, On the accuracy of the finite volume approximations to nonlocal conservation laws, Numer. Math., 156 (2024), pp. 237–271.
- [3] A. AGGARWAL AND G. VAIDYA, Convergence of the Numerical Approximations and Well-Posedness: Nonlocal Conservation Laws with Rough Flux, preprint, arXiv:2307.15153, 2023.
- [4] P. AMORIM, R. M. COLOMBO, AND A. TEIXEIRA, On the numerical integration of scalar nonlocal conservation laws, ESAIM Math. Model. Numer. Anal., 49 (2015), pp. 19–37.
- [5] F. Berthelin and P. Goatin, Regularity results for the solutions of a non-local model of traffic flow, Discrete Contin. Dyn. Syst., 39 (2019), pp. 3197–3213, https://doi.org/10.3934/ dcds.2019132.
- [6] F. BETANCOURT, R. BÜRGER, K. H. KARLSEN, AND E. M. TORY, On nonlocal conservation laws modelling sedimentation, Nonlinearity, 24 (2011), 855.
- [7] S. Blandin and P. Goatin, Well-posedness of a conservation law with non-local flux arising in traffic flow modeling, Numer. Math., 132 (2016), pp. 217–241.
- [8] Y. Brenier and S. Osher, The discrete one-sided Lipschitz condition for convex scalar conservation laws, SIAM J. Numer. Anal., 25 (1988), pp. 8–23.
- [9] A. Bressan and W. Shen, Entropy Admissibility of the Limit Solution for a Nonlocal Model of Traffic Flow, preprint, arXiv:2011.05430, 2020.
- [10] A. Bressan and W. Shen, On traffic flow with nonlocal flux: A relaxation representation, Arch. Ration. Mech. Anal., 237 (2020), pp. 1213–1236.
- [11] R. BÜRGER, P. GOATIN, D. INZUNZA, AND L. M. VILLADA, A non-local pedestrian flow model accounting for anisotropic interactions and walking domain boundaries, Math. Biosci. Eng., 17 (2020), pp. 5883–5906.
- [12] C. CHALONS, P. GOATIN, AND L. M. VILLADA, High-order numerical schemes for onedimensional nonlocal conservation laws, SIAM J. Sci. Comput., 40 (2018), pp. A288–A305, https://doi.org/10.1137/16m110825x.
- [13] F. A. CHIARELLO, P. GOATIN, AND E. ROSSI, Stability estimates for non-local scalar conservation laws, Nonlinear Anal. Real World Appl., 45 (2019), pp. 668–687, https://doi.org/10.1016/j.nonrwa.2018.07.027.

- [14] G. M. COCLITE, M. COLOMBO, G. CRIPPA, N. DE NITTI, A. KEIMER, E. MARCONI, L. PFLUG, AND L. V. SPINOLO, Oleinik-type Estimates for Nonlocal Conservation Laws and Applications to the Nonlocal-to-Local Limit, preprint, arXiv:2304.01309, 2023.
- [15] G. M. COCLITE, J.-M. CORON, N. DE NITTI, A. KEIMER, AND L. PFLUG, A general result on the approximation of local conservation laws by nonlocal conservation laws: The singular limit problem for exponential kernels, Ann. Inst. H. Poincaré C, (2022), pp. 1205–1223.
- [16] M. COLOMBO, G. CRIPPA, M. GRAFF, AND L. V. SPINOLO, On the role of numerical viscosity in the study of the local limit of nonlocal conservation laws, ESAIM Math. Model. Numer. Anal., 55 (2021), pp. 2705–2723.
- [17] M. COLOMBO, G. CRIPPA, E. MARCONI, AND L. V. SPINOLO, Local limit of nonlocal traffic models: Convergence results and total variation blow-up, Ann. Inst. H. Poincaré C Anal. Non Linéaire, 38 (2021), pp. 1653–1666.
- [18] M. COLOMBO, G. CRIPPA, E. MARCONI, AND L. V. SPINOLO, Nonlocal traffic models with general kernels: Singular limit, entropy admissibility, and convergence rate, Arch. Ration. Mech. Anal., 247 (2023), 18.
- [19] M. COLOMBO, G. CRIPPA, AND L. V. SPINOLO, On the singular local limit for conservation laws with nonlocal fluxes, Arch. Ration. Mech. Anal., 233 (2019), pp. 1131–1167.
- [20] R. M. COLOMBO, M. GARAVELLO, AND M. LÉCUREUX-MERCIER, A class of nonlocal models for pedestrian traffic, Math. Models Methods Appl. Sci., 22 (2012), 1150023.
- [21] R. M. COLOMBO AND E. ROSSI, Nonlocal conservation laws in bounded domains, SIAM J. Math. Anal., 50 (2018), pp. 4041–4065.
- [22] Q. Du, J. R. Kamm, R. B. Lehoucq, and M. L. Parks, A new approach for a nonlocal, nonlinear conservation law, SIAM J. Appl. Math., 72 (2012), pp. 464-487.
- [23] L. C. Evans and R. F. Garzepy, Measure Theory and Fine Properties of Functions, Routledge, New York, 2018.
- [24] F. FILBET AND S. JIN, A class of asymptotic-preserving schemes for kinetic equations and related problems with stiff sources, J. Comput. Phys., 229 (2010), pp. 7625–7648.
- [25] J. FRIEDRICH, S. GÖTTLICH, AND M. HERTY, Lyapunov stabilization for nonlocal traffic flow models, SIAM J. Control Optim., 61 (2023), pp. 2849–2875.
- [26] J. FRIEDRICH, S. GÖTTLICH, A. KEIMER, AND L. PFLUG, Conservation Laws with Nonlocal Velocity—The Singular Limit Problem, preprint, arXiv:2210.12141, 2022.
- [27] J. FRIEDRICH AND O. KOLB, Maximum principle satisfying CWENO schemes for nonlocal conservation laws, SIAM J. Sci. Comput., 41 (2019), pp. A973–A988.
- [28] J. FRIEDRICH, O. KOLB, AND S. GÖTTLICH, A Godunov type scheme for a class of LWR traffic flow models with non-local flux, Netw. Heterog. Media, 13 (2018), pp. 531–547.
- [29] J. FRIEDRICH, S. SUDHA, AND S. RATHAN, Numerical schemes for a class of nonlocal conservation laws: A general approach, Netw. Heterog. Media, 18 (2023), pp. 1335–1354, https://doi.org/10.3934/nhm.2023058.
- [30] P. GOATIN AND E. ROSSI, Well-posedness of IBVP for 1D scalar non-local conservation laws, ZAMM Z. Angew. Math. Mech., 99 (2019), e201800318.
- [31] P. GOATIN AND S. SCIALANGA, Well-posedness and finite volume approximations of the LWR traffic flow model with non-local velocity, Netw. Heterog. Media, 11 (2016), pp. 107–121.
- [32] E. Godlewski and P.-A. Raviart, Numerical Approximation of Hyperbolic Systems of Conservation Laws, Appl. Math. Sci. 118, Springer Science & Business Media, New York, 2013.
- [33] S. GÖTTLICH, S. HOHER, P. SCHINDLER, V. SCHLEPER, AND A. VERL, Modeling, simulation and validation of material flow on conveyor belts, Appl. Math. Model., 38 (2014), pp. 3295–3313.
- [34] K. Huang and Q. Du, Stability of a nonlocal traffic flow model for connected vehicles, SIAM J. Appl. Math., 82 (2022), pp. 221–243.
- [35] S. Jin, Efficient asymptotic-preserving (AP) schemes for some multiscale kinetic equations, SIAM J. Sci. Comput., 21 (1999), pp. 441–454.
- [36] S. Jin, Asymptotic Preserving (AP) Schemes for Multiscale Kinetic and Hyperbolic Equations: A Review, Lecture Notes for Summer School on Methods and Models of Kinetic Theory (M&MKT), Porto Ercole, Grosseto, Italy, 2010, pp. 177–216.
- [37] I. KARAFYLLIS, D. THEODOSIS, AND M. PAPAGEORGIOU, Analysis and control of a non-local PDE traffic flow model, Internat. J. Control, (2020), pp. 1–34, https://doi.org/10.1080/ 00207179.2020.1808902.
- [38] A. KEIMER AND L. PFLUG, On approximation of local conservation laws by nonlocal conservation laws, J. Math. Anal. Appl., 475 (2019), pp. 1927–1955.
- [39] A. KEIMER AND L. PFLUG, On the singular limit problem for a discontinuous nonlocal conservation law, Nonlinear Anal., 237 (2023), 113381.

- [40] R. KRYSTEK, Syntetyczny wskaźnik jakości ruchu ulicznego, Gdańsk University of Technology, Gdańsk, Poland, 1980.
- [41] R. J. LEVEQUE, Finite Volume Methods for Hyperbolic Problems, Cambridge Texts Appl. Math. 31, Cambridge University Press, Cambridge, 2002.
- [42] M. J. LIGHTHILL AND G. B. WHITHAM, On kinematic waves II. A theory of traffic flow on long crowded roads, Proc. A, 229 (1955), pp. 317–345.
- [43] O. OLEINIK, Discontinuous solutions of nonlinear differential equations, Amer. Math. Soc. Trans., 26 (1963), pp. 95–172.
- [44] P. I. RICHARDS, Shock waves on the highway, Oper. Res., 4 (1956), pp. 42-51.
- [45] J. RIDDER AND W. SHEN, Traveling waves for nonlocal models of traffic flow, Discrete Contin. Dyn. Syst., 39 (2019), 4001.
- [46] A. Romanowska and K. Jamroz, Comparison of traffic flow models with real traffic data based on a quantitative assessment, Appl. Sci., 11 (2021), 9914.
- [47] E. ROSSI, J. WEISSEN, P. GOATIN, AND S. GÖTTLICH, Well-posedness of a non-local model for material flow on conveyor belts, ESAIM Math. Model. Numer. Anal., 54 (2020), pp. 679–704.
- [48] W. Shen, Traveling waves for conservation laws with nonlocal flux for traffic flow on rough roads, Netw. Heterog. Media, 14 (2019), pp. 709-732.
- [49] E. TADMOR, The large-time behavior of the scalar, genuinely nonlinear Lax-Friedrichs scheme, Math. Comp., 43 (1984), pp. 353–368.
- [50] Z.-H. TENG AND P. ZHANG, Optimal L1-rate of convergence for the viscosity method and monotone scheme to piecewise constant solutions with shocks, SIAM J. Numer. Anal., 34 (1997), pp. 959–978.
- [51] X. Tian and Q. Du, Asymptotically compatible schemes and applications to robust discretization of nonlocal models, SIAM J. Numer. Anal., 52 (2014), pp. 1641–1665.
- [52] X. Tian and Q. Du, Asymptotically compatible schemes for robust discretization of parametrized problems with applications to nonlocal models, SIAM Rev., 62 (2020), pp. 199–227.
- [53] R. T. UNDERWOOD, Speed, volume and density relationships, in quality and theory of traffic flow, in Bureau of Highway Traffic, Yale University, New Haven, CT, 1961, pp. 141–188.